HHS Public Access

Author manuscript

Nat Biotechnol. Author manuscript; available in PMC 2024 June 18.

Published in final edited form as:

Nat Biotechnol. 2023 July ; 41(7): 944–957. doi:10.1038/s41587-022-01561-2.

A genetically encoded sensor measures temporal oxytocin release from different neuronal compartments

Tongrui Qian[1,2,13], **Huan Wang**[1,2,13], **Peng Wang**[3,13], **Lan Geng**[1,2], **Long Mei**[4], **Takuya Osakada**[4], **Lei Wang**[1,2,5], **Yan Tang**[6], **Alan Kania**[7], **Valery Grinevich**[7], **Ron Stoop**[6], **Dayu Lin**[4], **Minmin Luo**[8,9,10], **Yulong Li**[1,2,9,11,12]

[1]State Key Laboratory of Membrane Biology, Peking University School of Life Sciences, Beijing, China.

[2]PKU-IDG/McGovern Institute for Brain Research, Beijing, China.

[3]Medical Center for Human Reproduction, Beijing Chao-Yang Hospital, Capital Medical University, Beijing, China.

[4]Neuroscience Institute, Department of Psychiatry, New York University Grossman School of Medicine, New York, NY, USA.

[5]Peking University–Tsinghua University–National Institute of Biological Sciences Joint Graduate Program, Peking University, Beijing, China.

[6]Center for Psychiatric Neuroscience, Department of Psychiatry, Lausanne University Hospital Center (CHUV) and University of Lausanne (UNIL), Lausanne, Switzerland.

[7]Department of Neuropeptide Research in Psychiatry, Central Institute of Mental Health, Medical Faculty Mannheim, University of Heidelberg, Mannheim, Germany.

[8]National Institute of Biological Sciences (NIBS), Beijing, China.

[9]Chinese Institute for Brain Research, Beijing, China.

Correspondence and requests for materials should be addressed to Yulong Li. yulongli@pku.edu.cn.

Author contributions

Y.L. supervised the project. H.W. and L.G. performed the experiments related to the development, optimization and characterization of the sensors in cultured cells. T.Q. performed the two-photon imaging of OT dynamics in acute brain slices. L.W. performed the immunostaining experiments in brain slices. L.M., T.O. and A.K. performed the in vivo ICV infusion experiments in mice and rats under the supervision of D.L. and V.G. P.W. performed the in vivo fiber photometry recording and optogenetic experiments in mice under the supervision of M.L. Y.T. performed the optogenetic experiments in rats under the supervision of R.S. All authors contributed to the interpretation and analysis of the data. T.Q. and Y.L. wrote the manuscript with input from all authors.

Code availability

The custom-written ImageJ macro, MATLAB code and Arduino programs used in this study are available at https://github.com/OTsensor/2-photon_imaging_analysis, https://github.com/OTsensor/csv2xls and https://github.com/OTsensor/elec_stim_arduino.

Competing interests

Y.L. and H.W. have filed patent applications whose value might be affected by this publication. The remaining authors declare no competing interests.

Additional information

Extended data is available for this paper at https://doi.org/10.1038/s41587-022-01561-2.

Supplementary information The online version contains supplementary material available at https://doi.org/10.1038/s41587-022-01561-2.

[10]Tsinghua Institute of Multidisciplinary Biomedical Research (TIMBR), Tsinghua University, Beijing, China.

[11]Peking–Tsinghua Center for Life Sciences, Academy for Advanced Interdisciplinary Studies, Peking University, Beijing, China.

[12]National Biomedical Imaging Center, Peking University, Beijing, China.

[13]These authors contributed equally: Tongrui Qian, Huan Wang, Peng Wang.

Abstract

Oxytocin (OT), a peptide hormone and neuromodulator, is involved in diverse physiological and pathophysiological processes in the central nervous system and the periphery. However, the regulation and functional sequences of spatial OT release in the brain remain poorly understood. We describe a genetically encoded G-protein-coupled receptor activation-based (GRAB) OT sensor called $GRAB_{OT1.0}$. In contrast to previous methods, $GRAB_{OT1.0}$ enables imaging of OT release ex vivo and in vivo with suitable sensitivity, specificity and spatiotemporal resolution. Using this sensor, we visualize stimulation-induced OT release from specific neuronal compartments in mouse brain slices and discover that N-type calcium channels predominantly mediate axonal OT release, whereas L-type calcium channels mediate somatodendritic OT release. We identify differences in the fusion machinery of OT release for axon terminals versus somata and dendrites. Finally, we measure OT dynamics in various brain regions in mice during male courtship behavior. Thus, $GRAB_{OT1.0}$ provides insights into the role of compartmental OT release in physiological and behavioral functions.

Neuronal communication is typically described as a unidirectional process in which dendrites receive and integrate input information and the soma transforms the signals into action potentials, which then propagate to the axon terminal to release neurotransmitters. However, in addition to classical axonal release, some neurochemicals, such as GABA (γ-aminobutyric acid)[1], dopamine[2] and neuropeptides[3–5], also undergo somatodendritic release to reciprocally modulate surrounding neurons and regulate important physiological functions[6,7]. Evolutionarily ancient magnocellular neurosecretory cells (MNCs) in the paraventricular (PVN) and supraoptic (SON) nuclei of the hypothalamus have contributed extensively to the understanding of neurosecretory mechanisms, having been shown to release oxytocin (OT) or arginine vasopressin (AVP) from both the axonal and somatodendritic compartments[5,8,9].

OT is known to regulate a range of physiological processes in both the periphery and the central nervous system. In the mammalian brain, OT is produced by neurons located primarily in the PVN, SON and accessory nuclei of the hypothalamus[10]. The OT synthesized in these brain regions is released into the blood circulation from the posterior pituitary to serve as a hormone, regulating parturition and lactation via OT receptors (OTRs) that are robustly expressed in the uterus and mammary glands, respectively[11,12]. Apart from projecting to the pituitary, OT neurons send axons throughout the brain where axon-released OT modulates food intake, fear, aggression, social, sexual and maternal behaviors in rodents[13], while somatodendritic OT release has been associated with autocrine functions

during milk ejection and uterine contraction[14]. Coincident with the various physiological roles of OT, altered regulation of OT signaling has been associated with various negative emotional states and conditions such as stress, social amnesia, autism spectrum disorder and schizophrenia[15–18].

Not only does compartmental OT release display distinct functions, but somatodendritic OT release can also be primed by mobilization of intracellular Ca^{2+}, which has no reported effect on axonal OT release[5]. Thus, OT is likely to be released independently from each compartment. However, the molecular mechanisms underlying the compartmental control of OT release are largely unknown, even though several methods have already been developed to measure OT release. For example, microdialysis has been used for decades to monitor extracellular OT in freely moving animals[19–21]. Cell-based OT detection[22] uses exogenous 'sniffer cells' expressing OTRs to 'sniff' OT and reports it with increased intracellular Ca^{2+} levels. The recently developed genetically encoded OT sensor OTR-iTango2 measures downstream signals using light-induced activation of reporter gene expression[23], and the fluorescent OT sensor $MTRIA_{OT}$ has been reported[24]. However, these approaches do not provide tools for sensitive, specific and noninvasive monitoring of OT dynamics at high temporal and spatial resolution.

To address this need, we developed a highly sensitive OT-specific G-protein-coupled receptor (GPCR) activation-based (GRAB) sensor. We used this sensor ex vivo to identify the mechanisms of OT release in distinct cellular compartments. We also imaged the sensor in behaving mice and found region-specific OT release during discrete aspects of mating behaviors in male mice. Together, this work expands the toolbox of genetically encoded sensors for neurotransmitters and neuromodulators[25–35] to elucidate mechanisms of peptidergic signaling in the brain.

Results

Development and in vitro characterization of a $GRAB_{OT}$ sensor

To measure the dynamics of extracellular OT with high temporal and spatial resolution, we designed a genetically encoded GRAB sensor specific for OT ($GRAB_{OT}$). In this sensor, the circularly permutated GFP (cpGFP), which is flanked by linker peptides derived from the well-characterized $GRAB_{NE1m}$ norepinephrine sensor[28], serves as the fluorescent module, while the OTR functions as the ligand-recognition module (Fig. 1a). First, we systematically screened OTRs derived from ten vertebrate species (human, mouse, rat, bovine, sheep, pig, cat, chicken, monkey and medaka) by inserting the fluorescent module into the third intracellular loop (ICL_3) of each OTR with various insertion sites; we then measured each sensor's change in fluorescence ($\Delta F/F_0$) in response to OT (Fig. 1b). We selected the bovine OTR (bOTR)-based sensor (which we called $GRAB_{OT0.5}$) for further optimization because of its large change in fluorescence intensity following OT application. We then screened approximately 300 variants of $GRAB_{OT0.5}$ with different ICL_3 lengths, resulting in the optimized $GRAB_{OT1.0}$ sensor (hereafter referred to as OT1.0) with the highest response to OT and specific membrane targeting (Fig. 1c and Extended Data Fig. 1a). When we expressed OT1.0 in HEK293T cells, we found that bath application of OT induced a robust, stable response that was abolished by pretreating cells with the OTR antagonist atosiban,

but was not affected by the cholecystokinin B receptor antagonist YM022 (Extended Data Fig. 1b). For use as a negative control, we also developed an OT-insensitive variant called OTmut, which traffics to the plasma membrane but does not respond to OT (Extended Data Fig. 1d–f).

When expressed in cultured rat cortical neurons, OT1.0 was present throughout the plasma membrane, including in the soma and neurites (Fig. 1d). Following application of a saturating concentration of OT, both the soma and neurites displayed a robust increase in fluorescence, which was prevented by pretreatment with atosiban (Fig. 1d,e). We also measured the dose–response curve for OT1.0 expressed in neurons, with 3 nM OT eliciting the half-maximal effect ($EC_{50} \approx 3$ nM; Fig. 1f). OT1.0 had high specificity for OT, whose EC_{50} value was ~12-fold lower than that of AVP (Extended Data Fig. 1f), and had virtually no response to a wide range of other neurotransmitters and mammalian neuropeptides when expressed in cultured HEK293T cells (Extended Data Fig. 1h) or cortical neurons (Fig. 1g). Moreover, OT1.0 could potentially be used to monitor the OT orthologs of other species, including vasotocin (a nonmammalian AVP-like hormone) and isotocin (an OT homolog in fish), which had slightly higher EC_{50} values than OT(Extended Data Fig. 1g). Next, we examined whether the OT1.0 sensor had a response that was sufficiently rapid to capture OT applied using a local puffing system combined with high-speed line scanning. We found that OT1.0 had rapid response kinetics, with an average rise time constant (τ_{on}) of 480 ± 84 ms (Fig. 1h), and we estimated a rate constant for OT of $k_{on} = 69\ s^{-1}\ \mu M^{-1}$ for OT1.0 (Extended Data Fig. 1i–m). We then characterized the spectral properties of OT1.0 expressed in HEK293T cells before and after OT application and measured the peak excitation and emission wavelengths to be 505 nm and 520 nm, respectively (Extended Data Fig. 1c).

To confirm that the OT1.0 sensor does not couple to the downstream signaling pathways (and therefore does not affect cellular physiology), we used the Tango GPCR assay[36] to measure β-arrestin activation (Extended Data Fig. 2d). When expressed in HTLA cells (a HEK293T-derived cell line expressing a tetracycline-controlled trans-activator (tTA)-dependent luciferase reporter and a β-arrestin2–TEV fusion protein), OT1.0 had minimal β-arrestin coupling in response to OT; in contrast, wild-type bOTR displayed robust coupling (Extended Data Fig. 2d). Notably, OT1.0 did not interfere with signaling via wild-type bOTR, as cells coexpressing OT1.0 and bOTR had the same response to OT as cells expressing bOTR alone (Extended Data Fig. 2d). Moreover, there was no detectable coupling from OT1.0 to the G_q-dependent calcium signaling at defined OT concentrations[11,37] compared to wild-type bOTR (Extended Data Fig. 2a–c). Finally, we found that the OT response measured in OT1.0-expressing neurons was extremely stable for up to 120 min, indicating that the sensor undergoes negligible internalization or desensitization and can be used for long-term imaging of OT (Extended Data Fig. 2e). Taken together, these results confirm that the OT1.0 sensor can be used in vitro to measure extracellular OT with high sensitivity, high specificity and rapid kinetics.

Compartmental OT release measured in acute brain slices

Having shown that our OT1.0 sensor can be used in cultured cells, we next examined whether it could be applied to monitor endogenous OT release from oxytocinergic neurons in acute brain slices. We therefore injected adeno-associated viruses (AAVs) encoding OT1.0 (hSyn-OT1.0) and Cre-dependent excitatory G_q-DREADDs (EF1α-DIO-hM3Dq-mCherry) into the PVN of heterozygous OT-Cre mice (Extended Data Fig. 3a). After 3 weeks (to allow sufficient sensor expression), we found that activation of oxytocinergic neurons by bath application of the hM3Dq ligand deschloroclozapine (DCZ)[38] elicited a robust increase in OT1.0 fluorescence in the PVN, with a stronger response elicited by direct application of OT (Extended Data Fig. 3b,c). In contrast, DCZ elicited virtually no OT1.0 response in slices not expressing hM3Dq, while OT application still produced a peak response comparable to that in slices expressing hM3Dq (Extended Data Fig. 3b–d). Thus, OT1.0 can report the OT released from activated OT neurons.

We next tested whether OT1.0 can detect the dynamics of compartmental OT release in acute brain slices. PVN-originating OT input to the ventral tegmental area (VTA) has been shown to regulate social behavior via OT/OTR-mediated modulation of dopaminergic neurons[39–41]. Therefore, we injected a virus expressing either OT1.0 or OTmut under the control of the hSyn promotor into the VTA to visualize axonal OT release. After at least 3 weeks, acute sagittal brain slices containing the VTA region were prepared and used for two-photon imaging (Fig. 1i). We found that electrical stimulation delivered at 20 Hz evoked a progressively larger fluorescence increase in OT1.0, which was eliminated by treating slices with the OTR antagonist L368 (Fig. 1j,k). Moreover, no response was measured in slices expressing OTmut (Fig. 1i,k). We also measured the kinetics of axonal OT release in response to 20, 50 and 100 pulses delivered at 20 Hz and estimated the rise time constant (τ_{on}) and decay time constant (τ_{off}) at 1.3–3.2 s and 6.6–9.9 s, respectively (Fig. 1l).

In comparison to OT axons in the VTA, the PVN harbors the somatodendritic part of OT cells (Extended Data Fig. 4). To measure somatodendritic OT release, we expressed OT1.0 under the control of the hSyn promotor in the PVN and observed robust electrical stimulation-induced responses, which had rise time and decay time constants (τ_{on} and τ_{off}) of 3.0–4.0 s and 9.2–16.7 s, respectively, and were blocked by L368 (Fig. 1m–p). Such responses were absent in slices expressing OTmut (Fig. 1m,o). Electrical stimulation elicited no or little response of OT1.0 in the somatosensory cortex (S1) or dorsal striatum (dStr) compared to the response in the PVN (Extended Data Fig. 5). In addition, bath application of 100 nM OT elicited a robust fluorescence increase in OT1.0 in both PVN-containing slices (Extended Data Fig. 6a,f,g,i) and VTA-containing slices (Extended Data Fig. 6b,d,e,h), with only a slight response to 100 nM AVP (~16% of peak $\Delta F/F_0$ compared to OT) measured in the VTA (Extended Data Fig. 6c).

Spatial and temporal analysis of compartmental OT release

Although release of neuropeptides from large dense-core vesicles (LDCVs) is believed to occur on a much slower time scale than release of classic neurotransmitters from synaptic vesicles (SVs)[42], the precise spatial and temporal dynamics remain unclear. Therefore, we next compared the spatial and temporal kinetics of axonal and somatodendritic OT release

as well as glutamate release, using the OT1.0 sensor and iGluSnFR[43], a genetically encoded glutamate sensor, respectively. Applying a standard train of electrical stimulation to acute brain slices (measured in the VTA and PVN) elicited an OT1.0 fluorescence response with slower kinetics (τ_{on} of 2.6–2.7 s and τ_{off} of 8.5–12.7 s) in comparison to the iGluSnFR response (measured in the PVN, with τ_{on} of 0.3 s and τ_{off} of 3.4 s) (Fig. 2a,b,f). We then quantified $\Delta F/F_0$ at various distances from the release center and at various time points after the onset of stimulation and found that OT elicited a longer-lasting signal and diffused over a greater distance in comparison to glutamate (Fig. 2c,d,g). The apparent diffusion coefficients were approximately 5×10^3 μm^2 s^{-1} for OT in both the VTA and PVN, compared to 25.1×10^3 μm^2 s^{-1} for glutamate in the PVN (Fig. 2e,h). Our observations are consistent with the absence of a specific, rapid mechanism for recycling and degrading OT at the synaptic cleft, indicating that OT released from the axonal and somatodendritic compartments can diffuse slowly in the extrasynaptic space, serving as a long-lasting neuromodulator.

OT release uses compartment-specific calcium channels

Our finding that activity-induced OT release had strikingly different kinetics than glutamate release suggests that release of these transmitters might be coupled to different release mechanisms such as different sources of Ca^{2+} influx. To test this hypothesis, we first measured OT and glutamate signals in acute brain slices in response to electrical stimulation in solutions containing different levels of Ca^{2+} (Fig. 3a). We found that both OT and glutamate were released in a Ca^{2+}-dependent manner, but with significantly different EC_{50} values (Fig. 3a,b). Specifically, OT release, particularly from the somatodendritic compartment, required higher concentrations of extracellular Ca^{2+}. This observation is in line with the high levels of neuronal activation and intracellular Ca^{2+} required for neuropeptide release[44].

Oxytocinergic neurons express several subtypes of voltage-gated Ca^{2+} channels (VGCCs), including P/Q, N, L and R types[45–49]. The VGCC subtypes that are engaged in activity-dependent OT release in the axonal or somatodendritic compartment remain largely unknown. We therefore examined which VGCC subtypes mediate axonal and somatodendritic OT release by sequentially treating slices containing either the VTA or PVN with blockers of specific VGCC subtypes and monitoring stimulation-induced OT release (Fig. 3c,e). We first confirmed that presynaptic glutamate release in the VTA and PVN was inhibited by blocking both P/Q-type and N-type VGCCs using ω-agatoxin IVA (ω-Agx) and ω-conotoxin GVIA (ω-CTx), respectively[50,51] (Fig. 3c,d,f and Extended Data Fig. 7c). Notably, we found that axonal OT release depends mainly on N-type VGCCs whereas somatodendritic OT release is supported by L-type VGCCs (Fig. 3c–f and Extended Data Fig. 7a,b). On the basis of this pharmacological dissection, we conclude that activity-induced release of OT is Ca^{2+} dependent and uses compartment-specific VGCC subtypes.

Activity-dependent OT release requires the SNARE complex

In neurons, SNARE (soluble *N*-ethylmaleimide-sensitive factor attachment receptor) complexes are essential for the release of neurotransmitter-containing SVs[52] and neuropeptide-containing LDCVs[53]. With respect to SV fusion, the classic SNARE complex has been studied in detail and consists of VAMP2 (ref. [54]; vesicle-associated membrane

protein 2, also known as synaptobrevin 2), SNAP25 (ref. [55]; synaptosome-associated protein, 25 kDa) and syntaxin-1 (ref. [56]). In contrast, the SNARE proteins mediating OT-containing LDCV fusion, with respect to different neuronal compartments, have not been fully characterized.

To characterize the SNARE proteins that mediate OT release, we expressed the light chain of botulinum toxin serotype A (BoNT/A)[55] in the PVN to specifically cleave SNAP25 and subsequently measured OT and glutamate release with the OT1.0 sensor and iGluSnFR, respectively, in either the VTA (Fig. 4a) or PVN (Fig. 4b,c). As expected, glutamate release evoked by 100 electrical pulses delivered at 20 Hz was reduced in BoNT/A-expressing PVN slices (Fig. 4c). Similarly, stimulation-induced OT release detected by the OT1.0 sensor was also significantly reduced in both VTA and PVN slices expressing BoNT/A (Fig. 4a,b), indicating that SNAP25 has a critical role in both axonal and somatodendritic OT release.

Next, we expressed the tetanus toxin light chain (TeNT) in the PVN to specifically cleave vesicle-associated membrane proteins 1–3 (VAMP1–VAMP3, also known as synaptobrevin 1–3)[54,57] and studied its effect on OT release in the VTA (Fig. 4d) and PVN (Fig. 4e) in a similar set of experiments. We found that TeNT expression significantly reduced axonal OT release in the VTA, and the reduction was rescued by coexpressing TeNT-insensitive VAMP2 (VAMP2vw) with TeNT (Fig. 4d). Notably, somatodendritic OT release was unaffected by TeNT expression in the PVN, even though glutamate release was significantly reduced (Fig. 4e), suggesting that VAMP2 does not serve as the principal VAMP protein in LDCV-mediated somatodendritic OT release. OT cell-specific TeNT expression significantly reduced axonal OT release while somatodendritic OT release was unaffected (Extended Data Fig. 8). Taken together, these results indicate that activity-dependent OT release requires the SNARE complex, with SNAP25 involved in both axonal and somatodendritic OT release, whereas VAMP2 is essential only for axonal OT release.

Optogenetically evoked compartmental OT release in vivo

To address whether the OT1.0 sensor can be used to detect changes in the OT level in vivo, we virally expressed the OT1.0 sensor in the bed nucleus of stria terminalis (BNST) and measured its fluorescence response to rising concentrations of OT injected intraventricularly (Fig. 5a). A clear dose-dependent increase in fluorescence was observed over a 1,000-fold concentration range, with the maximum response reaching over 100% $\Delta F/F_0$ (Fig. 5b,c). The increase in OT1.0 sensor fluorescence was shown to be dependent on OT binding as it was blocked by pre-injection with the OTR antagonist atosiban (Fig. 5d). Control animals expressing OTmut in the BNST showed no response to OT injection at any dosage (Fig. 5b,c). We further examined OT1.0 responses to AVP. In line with in vitro results and the natural selectivity of the OTR, the AVP-induced OT1.0 response was significantly lower than that with OT (Fig. 5e). Similarly, OT1.0 expressed in the PVN of female rats also responded to intraventricularly injected OT (Extended Data Fig. 9), indicating that the OT1.0 sensor could be used to study OT release across rodent species.

To test whether the OT1.0 sensor can detect endogenously released OT in vivo in mice, we expressed DIO–ChrimsonR–tdTomato[58] in oxytocinergic PVN neurons together with either OT1.0 or OTmut in the medial prefrontal cortex (mPFC) of OT-Cre mice. We

then optogenetically stimulated ChrimsonR-expressing cells in the PVN and measured OT1.0 sensor signal in the mPFC (Fig. 5f). We found that optogenetic stimulation of oxytocinergic PVN neurons with increasing numbers of light pulses delivered at 20 Hz evoked a time-locked, progressive increase in OT1.0 signal in the mPFC, which was blocked by intraperitoneal injection with the OTR antagonist L368 5 min before stimulation (Fig. 5g,h). No increase in signal was measured in mice expressing OTmut in the mPFC, even after 10 s of optogenetic PVN stimulation (Fig. 5g,h), indicating that OT release induces a reliable increase in OT1.0 fluorescence. The rise and decay time constants ($T_{1/2}$) of the observed OT-mediated OT1.0 signal were 1.1–2.2 s and 1.4–4.2 s, respectively (Fig. 5i). Similarly, optogenetic activation of oxytocinergic PVN somas (Extended Data Fig. 10a) or SON-projecting axons (Extended Data Fig. 10e) with increasing frequencies of light pulses elicited a progressive increase in OT1.0 signal in the PVN (Extended Data Fig. 10b,c) or SON (Extended Data Fig. 10f,g). Such responses were absent in rats during excitation at an isosbestic control wavelength (Extended Data Fig. 10b,c,f,g). The time constants ($T_{1/2}$) of the observed somatodendritic OT-mediated OT1.0 signal (measured in the PVN, with a rise time of 1.1–3.1 s and a decay time of 1.2–9.7 s) were similar to those for axonal OT (measured in the SON, with a rise time of 0.5–6.8 s and a decay time of 1.7–11.1 s) (Extended Data Fig. 10d,h). Taken together, these results confirm that the OT1.0 sensor can be used to measure compartmental OT release in vivo with high sensitivity, good specificity and rapid kinetics.

Compartmental OT release during male mouse mating behaviors

OT has been reported to have a role in male mating behaviors[59–65]. It has been shown to increase at the PVN, VTA, medial preoptic area of the hypothalamus (mPOA), spinal cord and other regions during male sexual behaviors to presumably regulate these behaviors via the OTR[65–68]. To study the dynamics of OT release during male mating behaviors, we performed fiber photometry recording of OT1.0 fluorescence in the VTA, PVN and mPFC and observed region-specific responses during distinct phases of behavior (Fig. 5j,k). In the VTA, OT1.0 fluorescence increased (with rise and decay time constants ($T_{1/2}$) of 2.7 s and 4.3 s, respectively) during the ejaculation stage, but not during sniffing or intromission (Fig. 5l–o and Supplementary Video 1). In contrast, OT1.0 signal in the PVN increased during intromission (with rise and decay time constants ($T_{1/2}$) of 0.4 s and 0.4 s, respectively), but not during sniffing or ejaculation (Fig. 5l–o and Supplementary Video 2). Finally, OT1.0 signal in the mPFC was detected during sniffing (with rise and decay time constants ($T_{1/2}$) of 0.5 s and 0.6 s, respectively) and during ejaculation (with rise and decay time constants ($T_{1/2}$) of 1.0 s and 2.8 s, respectively) (Fig. 5l–o and Supplementary Video 3). As a negative control, no change in fluorescence was observed during any of the mating behaviors in the VTA, PVN or mPFC of mice expressing OTmut (Fig. 5j,l–n), confirming that the signals measured in mice expressing OT1.0 were not movement artifacts. These results indicate that OT is transiently released in specific brain regions and from distinct neuronal compartments during specific mating stages, thereby encoding key information for specific features of sexual behavior.

Discussion

Here we report the development and characterization of a genetically encoded fluorescence indicator for monitoring extracellular OT both in vitro and in vivo. Our OT1.0 sensor has a wide dynamic range, good sensitivity and selectivity for OT in comparison to other neurotransmitters and neuropeptides, high spatial and temporal resolution, and negligible downstream coupling. In acute mouse brain slices, we show that OT1.0 can probe the release of OT from specific neuronal compartments, that is, axonal OT release in the VTA and somatodendritic OT release in the PVN. Using this tool, we identify differential molecular mechanisms underlying OT release from axonal and somatodendritic neuronal compartments. Finally, in a series of fiber photometry-based experiments in freely moving male mice, we show differential OT release in discrete brain regions during specific stages of mating behaviors, as summarized in Fig. 6.

In comparison to other methods for monitoring OT release, our OT1.0 sensor has several distinct advantages. First, OT1.0 has a higher temporal resolution ($\tau_{on} \approx 0.5$ s) compared to microdialysis and OTR-iTango2, which are limited by a slow sampling rate (>5 min) and delayed reporter gene expression (~48 h), respectively. Although fluorescent indicator protein-tagged neuropeptides, such as NPY–pHluorin[69], have been used to image LDCV-mediated peptide release, the relatively large fluorescent protein fused with the peptide renders precise spatiotemporal measurements of neuropeptide release difficult with this approach. Recently, Ino et al.[24] reported a fluorescent OT sensor called $MTRIA_{OT}$ based on the medaka OTR designed using a similar strategy as OT1.0. In comparison to $MTRIA_{OT}$, the OT1.0 sensor has faster temporal dynamics, making it potentially more suitable for in vivo applications.

AVP, similarly to OT, can also be released from the somatodendritic compartment of PVN neurons[70]. In the central nervous system, AVP and OT often show opposing roles, especially in the context of social anxiety and depression, and the balance between OT and AVP is important for maintaining a normal mental state[71]. OT1.0 has an approximately 12-fold-higher apparent affinity for OT than AVP when expressed in cultured cells (Extended Data Fig. 1f), which is similar to the affinity of native mouse[72], rat[73], porcine[74] and human[75] OTRs. Further efforts could be applied to improve selectivity for OT over AVP, and vice versa, by modifying the ligand-binding pockets of OT1.0. An OT indicator with even higher selectivity for OT over AVP is likely needed to help discriminate the specific functions of OT and AVP in the central nervous system.

Our ex vivo experiments showed that OT release from both the somatodendritic and axonal compartments is considerably slower than synaptic glutamate release, in line with the faster kinetics of the SV fusion process as compared to LDCVs[44]. Moreover, we showed that OT has a slower diffusion rate and diffuses over a greater distance than classic neurotransmitters such as glutamate, which is possibly due to its relatively high molecular weight. Notably, we found that somatodendritic OT release has slower kinetics in terms of both rise and decay times when compared to axonal OT release. This might be due to the positive feedback of OT onto OT neurons. Indeed, the OTR is expressed in the somas and dendrites of magnocellular oxytocinergic neurons[76], where it couples to the G_q protein to increase the

intracellular Ca^{2+} concentration, thereby facilitating further OT release[77]. In addition, this may possibly be caused by slower replenishing of the more distant axonal release sites as compared to the somatodendritic compartment[78]. Another possible mechanism that could cause different kinetics of somatodendritic and axonal OT release is the involvement of different VGCCs and/or Ca^{2+} sensors.

Moreover, we also showed here that different types of VGCCs mediate OT release predominantly from somatodendritic (L-type VGCCs) and axonal (N-type VGCCs) compartments and that both SNAP25 and VAMP2 are required for axonal OT release, whereas SNAP25—but not VAMP2—is required for somatodendritic OT release. The different regulation of VAMP2 in part provides evidence excluding a possible contribution of axonal OT release in the PVN. Altogether, the molecular differences noted can account for the unique kinetics of axonal versus somatodendritic OT release. While transcriptome data have shown that P/Q-type and N-type VGCCs, VAMP2 and SNAP25 are highly expressed in OT neurons[45,47,48,79], the expression patterns of these proteins are divergent between the axonal and somatodendritic compartments of MNCs[46,80]. With respect to VGCCs, electrophysiological studies have shown that OT neurons are sensitive to blockage of L-type VGCCs in the cell body[81], which is consistent with our results that L-type VGCCs mediate somatodendritic OT release. Here we showed that N-type VGCCs are linked to axonal OT release in the VTA. Previously, R-type VGCCs were identified as a key regulator of OT secretion in the posterior pituitary[82]. Taking these findings together, this suggests the existence of output-specific release mechanisms in the axonal projections of OT neurons. Among the SNARE proteins, VAMP2 and SNAP25 were identified in axonal terminals, but were not enriched in the somas or dendrites of OT neurons[80]. Corresponding to this finding, our data suggest that other isoforms of synaptobrevin, not VAMP2, might be involved in somatodendritic OT release.

We also demonstrated that OT1.0 is an ideal tool to study OT dynamics in vivo and showed that OT is released during distinct phases of male sexual behavior in the PVN containing cell bodies and dendrites of oxytocinergic neurons, as well as in the target regions of oxytocinergic neuron axons—the VTA and PFC. We observed that OT is specifically released in the PVN during intromission, in the PFC during sniffing and ejaculation, and in the VTA during ejaculation. In contradiction to our results, a microdialysis study found that the OT level increased in the PVN after ejaculation[83], which was possibly due to poor spatial or temporal resolution. This mating stage-specific OT release in distinct brain regions is likely a consequence of differential control of axonal versus somatodendritic OT release[6]. We speculate that compartmental OT release is a key mechanism underlying temporally and spatially precise OT actions during behaviors. In line with this hypothesis, it has been reported that somatodendritic OT release mediates bursting of OT neurons in lactating rats[21,84], providing a plausible mechanism by which somatodendritic OT release rapidly increases axonal OT secretion in the posterior pituitary.

Given that the PVN contains both magnocellular and parvocellular oxytocinergic neurons, with specific electrophysiological properties, sizes, transcriptomes and innervation patterns[41,45,85–89], it will be crucial to determine whether compartmentalized OT release occurs in all oxytocinergic neurons or specific subpopulations. We speculate that

somatodendritic OT release mainly occurs in magnocellular OT neurons, which have larger cell numbers and produce more OT peptide than parvocellular OT neurons in the PVN[6], while the neuronal subtype responsible for axonal OT release in the VTA of mice remains controversial[40,41].

It is likely that compartmentalized release is displayed by other neurochemicals, such as dynorphin and brain-derived neurotrophic factor[4,90]. The GRAB strategy proposed here can also be used to develop new sensors for other neuropeptides that bind to GPCRs and answer fundamental physiological questions on the diversity versus similarity of peptide release mechanisms under diverse homeostatic and/ or behavioral challenges occurring in various mammalian species, including primates. Furthermore, this strategy will be highly useful to disentangle the efficiency with which peripherally administered OT (and other peptides) pass through the blood–brain barrier[91] and subsequently affect human behavior[92,93], mitigating symptoms of mental diseases[94,95].

In conclusion, our OT1.0 sensor is a robust tool for studying OT functions under both physiological and pathophysiological conditions, and our finding that OT released from axonal and somatodendritic compartments is controlled by distinct and compartmentalized molecular mechanisms provides insights into the complex actions of neuropeptides.

Online content

Any methods, additional references, Nature Portfolio reporting summaries, source data, extended data, supplementary information, acknowledgements, peer review information; details of author contributions and competing interests; and statements of data and code availability are available at https://doi.org/10.1038/s41587-022-01561-2.

Methods

Cell lines

HEK293T cells were obtained from the American Type Culture Collection. Cells expressing specific transgenes were selected using 2 μg ml^{-1} puromycin (Sigma). The HTLA cell line stably expressing a tTA-dependent luciferase reporter and the gene encoding the β-arrestin2–TEV fusion was a generous gift from B.L. Roth (University of North Carolina School of Medicine). All cell lines were cultured in DMEM (Gibco) supplemented with 10% (vol/vol) FBS (Gibco) and 1% penicillin-streptomycin (Gibco) at 37 °C in 5% CO_2.

Primary neuronal cultures

Rat cortical neurons were cultured from postnatal day (P) 0 Sprague–Dawley rat pups of both sexes (Beijing Vital River). Specifically, the brain was removed and the cortex was dissected; neurons were then dissociated in 0.25% trypsin-EDTA (Gibco), plated on 12-mm glass coverslips coated with poly(D-lysine) (Sigma-Aldrich) and cultured in neurobasal medium (Gibco) containing 2% B-27 supplement, 1% GlutaMax (Gibco) and 1% penicillin-streptomycin (Gibco) at 37 °C in 5% CO_2.

Animals

P0 Sprague–Dawley rats of both sexes (Beijing Vital River), male adult (P42–P56) wild-type C57BL/6N mice (Beijing Vital River), male adult mice (Taconic) in the SW background, female adult Sprague–Dawley wild-type rats, male adult OT-IRES-Cre mice (Jackson Laboratory), male adult OT-knockout mice (Jackson Laboratory), and LSL-Cas9-tdTomato (GemPharmatech) and Ai14 (Jackson Laboratory) mice were used to prepare primary neuronal cultures and acute brain slices and/or for in vivo experiments. Animals were housed at 18–23 °C in 40–60% humidity under a 12-h light/12-h dark cycle, with food and water available ad libitum. All experimental protocols were approved by the respective Laboratory Animal Care and Use Committee of Peking University, the Chinese Institute for Brain Research, New York University, Lausanne University Hospital Center or the University of Heidelberg, and all studies were performed in accordance with the guidelines established by the National Institutes of Health.

Molecular cloning

DNA fragments were generated using PCR amplification with 20- to 30-bp primers (Tsingke Biological Technology). Plasmids were generated using the Gibson assembly method, and all plasmid sequences were verified using Sanger sequencing. All plasmids encoding the candidate OT sensors were cloned into the pDisplay vector (Invitrogen) with an upstream IgK leader sequence and a downstream IRES-mCherry-CAAX cassette for labeling the plasma membrane. cDNAs encoding the various OTRs were amplified from the human GPCR cDNA library, amplified from genomic DNA or synthesized (Shanghai Generay Biotech), and the ICL_3 of each OTR was swapped with the corresponding ICL_3 in the $GRAB_{NE}$ sensor. The plasmids for expressing the OT sensors in rat cortical neurons and mouse brain slices were cloned into the pAAV vector under the control of the human synapsin (hSyn) promoter. The sequences of the primers used in this study are listed in Supplementary Table 1.

Recombinant AAVs

AAV2/9-hSyn-OT1.0 (1.80×10^{13} genome copies per ml; CIBR vector core or WZ Biosciences), AAV2/9-hSyn-OTmut (4.59×10^{13} genome copies per ml; WZ Biosciences), AAV2/9-hSyn-iGluSnFR (SF.iGluS-nFR.A184V) (1.41×10^{13} genome copies per ml; WZ Biosciences), AAV2/9-EF1α-DIO-hM3Dq-mCherry (2.70×10^{12} genome copies per ml; BrainVTA), AAV2/9-CMV-BFP2-P2A-TeNT (1.54×10^{14} genome copies per ml; WZ Biosciences), AAV2/9-hSyn-jRGECO1a-P2A-VAM P2vw (2.02×10^{13} genome copies per ml; He Yuan Bioengineering), AAV2/9-hSyn-BFP2-P2A-BoNT/A (3.26×10^{13} genome copies per ml; He Yuan Bioengineering), AAV2/9-hSyn-DIO-PSD95-EGFP (9.10×10^{13} genome copies per ml; WZ Biosciences), AAV2/9-hEF1α-DIO-mCherry-P2A-TeNT (1.00×10^{13} genome copies per ml; Shanghai Taitool Bioscience) and AAV2/9-CAG-DIO-ChrimsonR-tdTomato (1.30×10^{13} genome copies per ml; Shanghai Taitool Bioscience) were used to infect cultured neurons or were injected into specific brain regions in mice.

Fluorescence imaging of cultured cells

An inverted confocal microscope (Nikon) equipped with NIS-Elements 4.51.00 software (Nikon), a ×40/1.35-NA oil-immersion objective, a 488-nm laser and a 561-nm laser was used for imaging; the GFP and RFP signals were collected using 525/50-nm and 595/50-nm emission filters, respectively. Cultured cells expressing OT1.0 or OTmut were either bathed or perfused with Tyrode's solution containing (in mM) 150 NaCl, 4 KCl, 2 $MgCl_2$, 2 $CaCl_2$, 10 HEPES and 10 glucose (pH 7.4); where indicated, drugs and other compounds were delivered via a custom-made perfusion system or via bath application. An Opera Phenix high-content screening system (PerkinElmer) equipped with a ×40/1.1-NA water-immersion objective, a 488-nm laser and a 561-nm laser was also used for imaging; the GFP and RFP signals were collected using 525/50-nm and 600/30-nm emission filters, respectively. The Harmony 4.9 software of the Opera Phenix high-content screening system (PerkinElmer) was used for data collection. For imaging, the fluorescence signals of the candidate OT sensors were calibrated using the GFP/RFP fluorescence ratio. To measure the response kinetics of the OT1.0 sensor, the line-scanning mode of the confocal microscope was used to record rapid changes in fluorescence; a glass pipette containing 10 μM OT was placed near the surface of HEK293T cells expressing the OT1.0 sensor, and OT was puffed onto cells to measure τ_{on}. To obtain the dose–response curves for the OT1.0 sensor shown in Fig. 1g and Extended Data Fig. 1c,d, solutions containing OT (ANASPEC or KS-V Peptide) or AVP (ANASPEC or KS-V Peptide), vasotocin (MedChem-Express), isotocin (MedChemExpress), inotocin (MedChemExpress) or nematocin (KS-V Peptide) with various concentrations were bath applied to OT1.0-or OTmut-expressing HEK293T cells and fluorescence was measured using the Opera Phenix high-content screening system (PerkinElmer).

Tango GPCR assay

The constructs encoding wild-type bOTR, OT1.0 or both were transfected into cells stably expressing a tTA-dependent luciferase reporter and the gene encoding the β-arrestin2–TEV fusion protein. After transfection, cells were bathed in culture medium supplemented with various concentrations of OT and then cultured for 12 h to allow expression of luciferase. The culture medium was then replaced with Bright-Glo reagent (Fluc Luciferase Assay System, Promega) at a final concentration of 5 μM, and luminescence was measured using a Victor468 X5 multilabel plate reader with Victor2030 Workstation software 4.0 (PerkinElmer).

Calcium imaging of cultured cells

bOTR-IRES-BFP or OT1.0-IRES-BFP plasmid was transfected into HEK293T cells. After transfection, cells were loaded with Cal590 (3 μg ml^{-1}; AAT Bioquest) for 50 min and consecutively perfused with solutions containing OT at various concentrations (0, 0.01, 0.1, 1 and 10 nM) and 100 μM ATP. The Ca^{2+} response was measured using a confocal microscope (Nikon).

Preparation and fluorescence imaging of mouse acute brain slices

Wild-type C57BL/6N mice or OT-Cre mice were deeply anesthetized by an intraperitoneal injection of avertin (500 mg kg^{-1}; Sigma-Aldrich) and then placed in a stereotaxic frame for injection of AAVs using a microsyringe pump (Nanoliter 2000 Injector, WPI). For the data shown in Fig. 2a–d, EF1α-DIO-hM3Dq-mCherry and/or hSyn-OT1.0 AAVs were injected (300 nl per site) into the left PVN of OT-Cre mice or OT-Cre × Ai14 mice using the following coordinates: anteroposterior (AP), −0.75 mm relative to bregma; mediolateral (ML), −1.5 mm; dorsoventral (DV), −4.95 mm from the dura; at a 15° angle. For the data shown in Figs. 2e–l and 3–5, the indicated AAVs were injected in C57BL/6N mice (300 nl per site) into either the PVN as described above or the VTA using the following coordinates: AP, −3.2 mm relative to bregma; ML, −0.5 mm; DV, −4.1 mm from the dura. For the data shown in Extended Data Fig. 4, the indicated AAVs were injected in C57BL/6J mice (300 nl per site) into either the S1 or the dStr using the following coordinates: S1: AP, −1.1 mm relative to bregma; ML, −3.1 mm; DV, −0.5 mm from the dura; dStr: AP, +0.8 mm relative to bregma; ML, −1.8 mm; DV, −3.3 mm from the dura.

Three weeks after viral injection, mice were again deeply anesthetized with an intraperitoneal injection of avertin and transcardial perfusion was performed using cold oxygenated slicing buffer containing (in mM) 110 choline chloride, 2.5 KCl, 1 NaH_2PO_4, 25 $NaHCO_3$, 7 $MgCl_2$, 25 glucose, 0.5 $CaCl_2$, 1.3 sodium ascorbate and 0.6 sodium pyruvate. Brains were then rapidly removed and immersed in the oxygenated slicing buffer, after which the cerebellum was trimmed using a razor blade. The brains were then glued to the cutting stage of a VT1200 vibratome (Leica) and sectioned into 300-μm-thick coronal slices. Brain slices containing the PVN or VTA were incubated at 34 °C for at least 40 min in oxygen-saturated Ringer's buffer containing (in mM) 125 NaCl, 2.5 KCl, 1 NaH_2PO_4, 25 $NaHCO_3$, 1.3 $MgCl_2$, 25 glucose, 2 $CaCl_2$, 1.3 sodium ascorbate and 0.6 sodium pyruvate. For two-photon imaging, the slices were transferred into an imaging chamber in an FV1000MPE (Olympus) or Ultima Investigator 2P (Bruker) microscope equipped with a ×25/1.05-NA water-immersion objective and a mode-locked Mai Tai Ti:Sapphire laser (Spectra-Physics) tuned to 920 nm with a 495- to 540-nm filter to measure fluorescence. FV10-ASW Ver.3.1a software for the FV1000MPE two-photon microscope (Olympus) and Prairie View 5.5 software for the Ultima Investigator two-photon microscope (Bruker) were used for data collection. For electrical stimulation, a homemade bipolar electrode (WE30031.0A3, MicroProbes) was placed onto the surface of the brain slice near the VTA or PVN under fluorescence guidance. Imaging and stimulation were synchronized using an Arduino board with a custom-written program. Experiments to probe the spatial and temporal kinetics of glutamate release were recorded at a video frame rate of 0.0171 s per frame, with 256 × 256 pixels per frame. All other stimulation experiments were recorded at video frame rates of 0.3583 or 0.3259 s per frame, with 256 × 192 or 256 × 256 pixels per frame. The stimulation voltage was set at 5–8 V, and the duration of each stimulation was 1 ms. Where applicable, drugs and other compounds were applied to the imaging chamber by perfusion in ACSF at a flow rate of 4 ml min^{-1}.

In vivo fiber photometry recording of OT1.0 responses during ICV infusion of drugs in mice

Adult wild-type male mice (Taconic) on the SW background were used for surgery. During surgery, mice were anesthetized with 1–2% isoflurane and mounted onto a stereotaxic device (Kopf Instruments, model 1900). Then, 500 nl AAV9-hSyn-OT1.0 or AAV9-hSyn-OTmut virus was delivered into the BNST (AP, −0.45 mm; ML, −0.9 mm; DV, −3.6 mm) through a glass capillary using a nanoinjector (Nanoliter 2000, WPI). After virus injection, a 400-μm optical fiber assembly (Thorlabs, FR400URT, CF440) was inserted 300 μm above the virus injection site and secured onto the skull using adhesive dental cement (C&B Metabond, S380); at the same time, a cannula was inserted into the right-side lateral ventricle and secured onto the skull using adhesive dental cement (C&B Metabond, S380). Three weeks after surgery, the mice were head-fixed on a running wheel and fluorescence signals of the sensor were acquired as described previously[96]. Mice were recorded for 25 min and subsequently infused ICV with various amounts (time interval between two trials of 24 h) of OT and AVP dissolved in 0.5 μl saline and recorded for an additional 25 min. The OTR antagonist atosiban (50 mM in 0.5 μl saline) was injected ICV 5 min before the OT infusion. Drug-induced responses were calculated as the mean fluorescence level after each drug injection minus the mean fluorescence level before drug injection.

In vivo fiber photometry recording of OT1.0 responses during ICV infusion of OT in rats

Adult female Sprague–Dawley rats were anesthetized with 2–4% isoflurane and mounted onto a stereotaxic frame (Kopf Instruments). Then, 500 nl of AAV9-hSyn-OT1.0 virus was delivered into the PVN (AP, −1.8 mm; ML, −0.35 mm; DV, −8 mm relative to bregma) using a glass microinjection pipettes connected to a syringe pump. At least 2 weeks after viral injection, rats were anesthetized again with isoflurane and mounted onto the stereotaxic frame. Optical fibers (400 μm) were placed above the PVN region (AP, −1.8 mm; ML, −2 mm; DV, −7.8 mm relative to bregma; at a 14° angle), while glass microinjector pipettes connected to a syringe pump were lowered into the lateral ventricle (AP, −0.7 mm; ML, 1.8 mm; DV, −4 mm relative to bregma). The fiber photometry experiment was performed using a bundle-imaging fiber photometry setup (Doric Lenses). OT1.0 was stimulated using 400- to 410-nm (isosbestic) and 460- to 490-nm excitation LEDs; fluorescence emitted at 500–550 nm was detected with a CMOS camera in inter-leaved acquisition mode. The signal was recorded for 3 min before ICV OT injection (1 μl, 10 mM) and for 20 min afterward. To verify the optical fiber placement and OT1.0 expression, selected rats were transcardially perfused with 100 ml saline followed by 100 ml of 4% formaldehyde in PBS. Postfixed brains were cut into coronal sections (50 μm) and analyzed with an epifluorescence microscope (Nikon). Sections were stained for GFP to visualize sensor expression.

In vivo fiber photometry recording of OT1.0 responses during optogenetic activation in rats

Adult female Sprague–Dawley rats were anesthetized with 2–4% isoflurane and mounted onto a stereotaxic frame. As described previously[97], an AAV encoding the promoter for the *Oxt* gene (pOT) driving ChrimsonR–tdTomato expression was injected into the PVN and

an AAV encoding hSyn-OT1.0 was injected into the PVN or SON of Sprague–Dawley rats using the following coordinates (PVN: AP, −1.8 mm; ML, 0.4 mm; DV, −8.0 mm relative to bregma; SON: AP, −1.2 mm; ML, 1.8 mm; DV, −9.2 mm relative to bregma); 3 weeks after virus injections, an optical fiber (400 μm, 0.5 NA) was implanted in the PVN or SON to activate OT neuron somas or axons and record OT release. For this purpose, it was coupled with a fiber patch cord (200 μm, 0.37 NA) and linked to an integrated fluorescence minicube (Doric, ilFMC5). The minicube was connected to a fluorescence detector head to record the 525-nm fluorescence emission signal and connected to a double-wavelength LED (20 μW mm^{-2}) to excite the OT1.0 sensor at an isosbestic control wavelength (405 nm) or OT-sensitive sensor wavelength (465 nm). In addition, it was connected to a 593-nm LED (10 mW mm^{-2}) to activate ChrimsonR through the same fiber core without bleedthrough into the 525-nm detection channel. Traces are the average response of 30 individual trials in the same rat; light color indicates the standard deviation.

In vivo fiber photometry recording of OT dynamics during optogenetic activation or sexual behavior

Adult male wild-type C57BL/6N (Beijing Vital River) or adult male OT-IRES-Cre (Jackson Laboratory) mice were deeply anesthetized with an intraperitoneal injection of avertin and then placed in a stereotaxic frame for AAV injection. For optogenetics, AAVs encoding hSyn-OT1.0 or hSyn-OTmut were injected (300 nl per site) into the left mPFC using the following coordinates: AP, +1.9 mm relative to bregma; ML, −0.3 mm; DV, −1.8 mm from the dura; in addition, an AAV encoding CAG-DIO-ChrimsonR-tdTomato was injected (300 nl per site) into the left PVN of male OT-IRES-Cre mice using the following coordinates: AP, −0.75 mm relative to bregma; ML, −1.5 mm; DV, −4.95 mm from the dura; at a 15° angle. Mice were treated with an intraperitoneal injection of either saline or L368 (Tocris, 10 mg kg^{-1}) 30 min before light stimulation. For the sexual behavior experiments involving wild-type male mice, AAVs encoding hSyn-OT1.0 or hSyn-OTmut were injected (300 nl per site) into the left VTA using the following coordinates: AP, −3.2 mm relative to bregma; ML, −0.5 mm; DV, −4.1 mm from the dura; the left PVN using the following coordinates: AP, −0.75 mm relative to bregma; ML, −1.5 mm; DV, −4.95 mm from the dura; at a 15° angle; or the left mPFC using the following coordinates: AP, +1.9 mm relative to bregma; ML, −0.3 mm; DV, −1.8 mm from the dura. Optical fibers (105-μm core/125-μm cladding) were implanted in the mPFC, VTA and/or PVN 3 weeks after AAV injection. A fiber photometry system (Thinker-biotech) was used to record signals in the mPFC, VTA and/or PVN using a 470-nm laser at 50 μW for OT1.0 or OTmut, and ChrimsonR expressed in the PVN was stimulated using a 593-nm laser at 10 mW (10-ms pulses were applied at 20 Hz for 0.25–10 s). A 535/50-nm filter was used to collect the fluorescence signal from OT1.0 or OTmut. The animal’s sexual behaviors were recorded using the commercial video acquisition software StreamPix 5 (Norpix), and behaviors were annotated and tracked using custom-written MATLAB code (MATLAB R2019a, MathWorks). After excluding mice with incorrect fiber placement, we analyzed 6 of 18 mice, 6 of 18 mice and 6 of 16 mice with a significant fluorescence change during mating behavior in the PVN, VTA and PFC, respectively.

Immunohistochemistry

To examine the somatodendrites of OT neurons, mice were anesthetized and perfused using 4% paraformaldehyde in PBS. After postfixation overnight, brains were sectioned at 40-μm thickness into coronal sections using a VT1200 vibratome (Leica). Sections were incubated with blocking solution (5% normal goat serum) for 1 h and then incubated with AGT (0.5% goat serum, 0.1% Triton X-100 and 2 mM $MgCl_2$ in PBS) containing primary antibodies overnight at 4 °C on an orbital shaker. The following day, brain sections were rinsed three time with AGT and then incubated with AGT containing secondary antibodies (1:2,000 dilution) for 2 h. The slices were then incubated in AGT containing DAPI (dilution 1:2,000; Sigma, 5 mg ml^{-1}, d9542) for 15 min. Finally, brain sections were washed three times with AGT and mounted onto slides. The following primary and secondary antibodies were used in the current study: rabbit anti-OT (G-051–01, Phoenix Pharma; 1:500 dilution), chicken anti-GFP (ab13970, Abcam; 1:1,000 dilution), iFluor 488 goat anti-rabbit IgG (H+L) (16678, AAT Bioquest), iFluor 647 goat anti-rabbit IgG (H+L) (16710, AAT Bioquest) and Alexa 488-conjugated goat anti-chicken IgG (H+L) (A11039, Invitrogen). The fluorescence images were captured using an epifluorescence microscope (VS120, Olympus).

Data analysis

Imaging data obtained from cultured cells and acute brain slices were processed using ImageJ software (NIH) with a custom-written macro. The change in fluorescence ($\Delta F/F_0$) was calculated using the formula $(F - F_0)/F_0$, in which F_0 is the baseline fluorescence signal. Statistical analyses were performed using GraphPad Prism 8.0. The two-tailed Student's *t* test or one-way ANOVA was performed where appropriate, and differences with a P value <0.05 were considered significant. Traces and summary graphs were generated using OriginPro 2020b (OriginLab). The cartoons in Fig. 6 and Extended Data Figs. 3a, 4b, 5a and 9a were created with BioRender.com.

Reporting summary

Further information on research design is available in the Nature Portfolio Reporting Summary linked to this article.

Extended Data

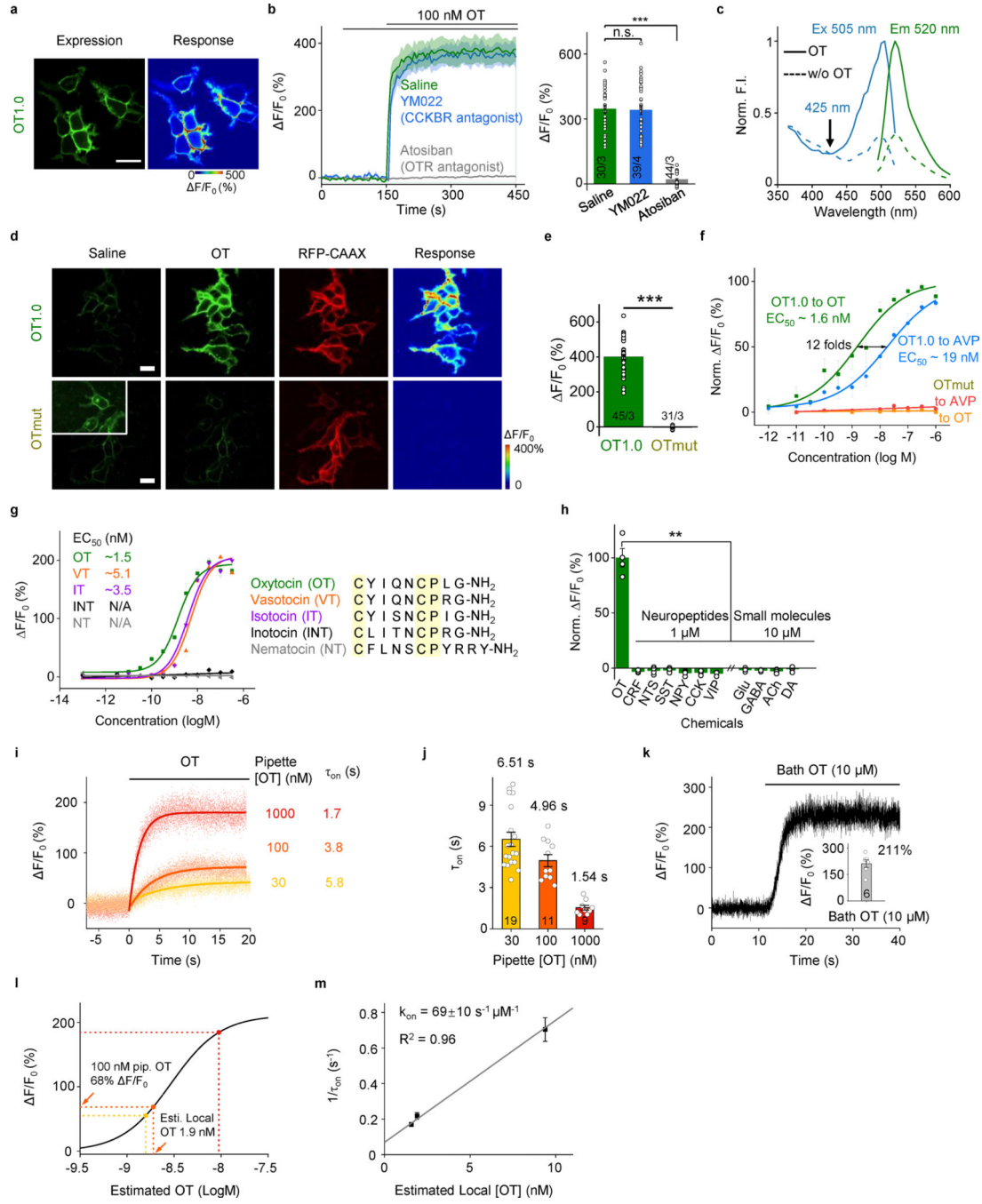

Extended Data Fig. 1 |. Characterization of GRAB$_{OT}$ sensors in HEK293T cells.

a. Representative expression and response images of OT1.0 to 100 nM OT in HEK293T cells. Scale bar, 20 μm. **b**. Example traces (left) and summary data (right) of OT1.0-expressing HEK293T cells pre-incubated with saline, 10 μM YM022, or 10 μM Atosiban in response to OT. Saline: n = 30 cells from 3 coverslips [30/3], YM022: n = 39/4, Atosiban: n = 44/3. Two-tailed Student's *t*-tests, p = 0.84 (between Saline and YM022); p = 9.8

$\times 10^{-18}$ (between Saline and Atosiban). **c**. Excitation (Ex) and emission (Em) spectra of the OT1.0 sensor with or without 100 nM OT. **d**. Representative images of OT1.0 and OTmut expressed in HEK293T cells in saline and in the presence of 100 nM OT. Also shown is RFP-CAAX expression, showing localization at the plasma membrane. The images at the right show the change in OT1.0 and OTmut fluorescence in response to OT application. White rectangle with enhanced contrast showing OTmut expressing HEK293T cells in saline. Scale bars, 20 μm. **e**. Summary of the peak change in OT1.0 and OTmut fluorescence measured in HEK293T cells in response to 100 nM OT. OT1.0: n = 45 cells from 3 coverslips; OTmut: n = 31 cells from 4 coverslips. Two-tailed Student's *t*-tests were performed ($p = 5.5 \times 10^{-31}$). **f**. Dose–response curves for OT1.0 and OTmut expressed in HEK293T cells in response to the indicated concentrations of OT and AVP, with the corresponding EC_{50} values shown. The data were normalized to the maximal response measured in OT group. The dosage curves of OT1.0 to OT/AVP were averaged from 9 individual trials, with 3–4 wells per trial. **g**. Dose-response curves for OT1.0 expressed in HEK293T cells in response to the indicated concentrations of OT and its orthologous peptides, with amino acid sequence alignment shown. n = 4 coverslips for each group. **h**. Summary of the peak change in OT1.0 fluorescence measured in HEK293T cells in response to the indicated compounds applied at 1 μM (CRF, NTS, NPY, and VIP) or 10 μM (Glu, GABA, Gly, DA, NE, and 5-HT), normalized to the peak response measured in OT; n = 4 wells per group. CRF, corticotropin-releasing factor; NTS, neurotensin; NPY, neuropeptide Y; VIP, vasoactive intestinal peptide; Glu, glutamate; GABA, γ-aminobutyric acid; Gly, glycine; DA, dopamine; NE, norepinephrine; and 5-HT, 5-hydroxytryptamine (serotonin). One-way ANOVA test was performed for all groups ($F(10, 3.88) = 132.3$, $p = 2.0 \times 10^{-4}$); Dunnett's T3 multiple comparisons tests were performed ($p = 4.6 \times 10^{-3}$, 3.8×10^{-3}, 4.4×10^{-3}, 4.0×10^{-3}, 4.2×10^{-3}, 4.2×10^{-3}, 4.6×10^{-3}, 4.8×10^{-3}, 4.5×10^{-3}, and 4.5×10^{-3} (between OT and CRF, NTS, SST, NPY, CCK, VIP, Glu, GABA, ACh, DA)). **i**. Representative traces of the OT1.0 signal evoked by OT puffing at indicated concentrations. **j**. Summary of the OT1.0 signal time constant at indicated OT concentrations ($n = 19$ cells for 30 nM OT, $n = 11$ cells for 100 nM OT and $n = 9$ cells for 1000 nM OT). **k**. Representative traces and summary $\Delta F/F_0$ of OT1.0 when bath application of OT at saturated concentration using line-scanning mode. $n = 6$ trials. **l**. The calibration curve of OT1.0 dose-dependent fluorescence response in line-scanning mode, which is used to estimate the local OT concentration reaching the cells during local puffing experiments. **m**. The association rate constant of the OT1.0 sensor for OT. Local OT concentrations were estimated from **i** ($n = 19$ cells for 30 nM OT, $n = 11$ cells for 100 nM OT and $n = 9$ cells for 1000 nM OT). $^{**}p < 0.01$, and $^{***}p < 0.001$. Summary data are presented as the mean±s.e.m.

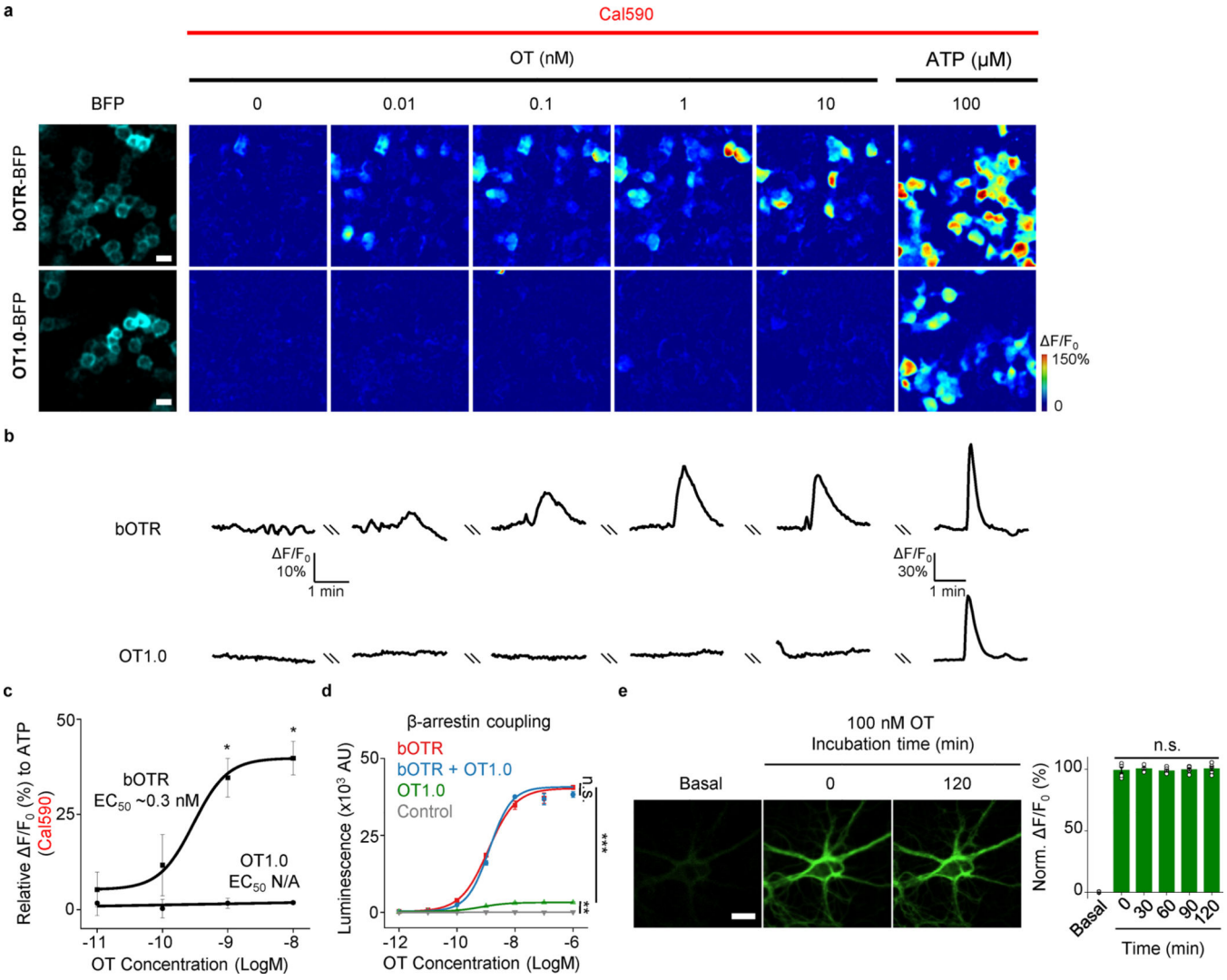

Extended Data Fig. 2 |. Negligible downstream signaling coupling of OT1.0 sensor in HEK293T cells.

a, **b**. Representative expression images in BFP channel, pseudocolor images (top) and $\Delta F/F_0$ traces (bottom) showing the Ca^{2+} response to the indicated concentrations of OT or ATP in HEK293T cells expressing bOTR-BFP (**a**) or OT1.0-BFP (**b**). **c**. Summary of peak Ca^{2+} $\Delta F/F_0$ for bOTR or OT1.0 expressed HEK293T cells corresponding to (**a** and **b**) at indicated OT concentrations, with the corresponding EC_{50} value shown. The data were normalized to the peak response measured in 100 μM ATP. n = 3 coverslips for each group. Two-tailed Student's *t*-tests were performed between bOTR and OT1.0 (p = 0.56, 0.29, 0.018, and 0.013 for 0.01, 0.1, 1, and 10 nM OT). **d**. β-arrestin coupling was measured using the Tango assay in cells expressing the bovine OTR (bOTR), OT1.0, bOTR and OT1.0, or no receptor (Control). n = 3 wells each. Two-tailed Student's *t*-tests, p = 0.12 (between bOTR and bOTR+OT1.0); $p = 6.8 \times 10^{-7}$ (between bOTR and OT1.0); $p = 2.9 \times 10^{-3}$ (between OT1.0 and Control). **e**. Representative images (left) and summary (right) of the fluorescence change in OT1.0-expressing neurons in response to a 2-hour continuous OT application. n = 5 cultures with >30 cells each. Row matched one-way ANOVA, with the Geisser-Greenhouse

correction, F (1.509,6.037) =0.16, p = 0.79. *p < 0.05, **p < 0.01, ***p < 0.001, and n.s., not significant. All scale bars represent 20 μm. Summary data are presented as the mean±s.e.m.

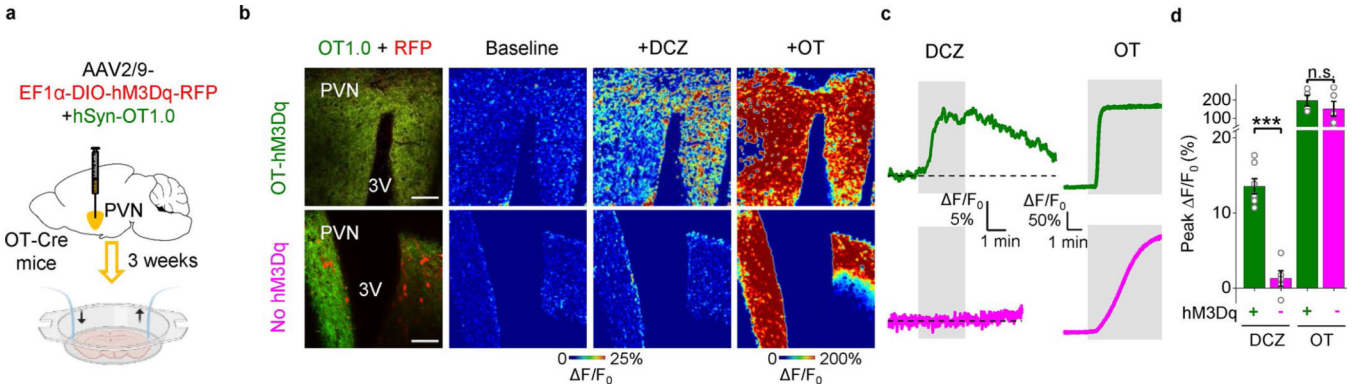

Extended Data Fig. 3 |. Chemogenetic activation of oxytocinergic neurons induces OT release. **a**. Schematic diagram depicting the chemogenetic activation experiments. A mixture of AAVs (EF1α-dio-hM3Dq-mCherry and hSyn-OT1.0) was injected into the PVN of OT-Cre mice. As a control, hSyn-OT1.0 was injected into the PVN of OT-Cre x Ai14 mice (no-hM3Dq). The PVN and third ventricle (3 V) are indicated. **b**. Left: representative 2-photon microscopy merged images of OT1.0 (green channel) and the RFP channel (red, mCherry expression for OT-hM3Dq and tdTomato for no-hM3Dq). Right: responses of the OT1.0 sensor measured in ACSF (baseline), 60 nM DCZ, and 100 nM OT. Scale bars, 100 μm. **c**, **d**. Example OT1.0 traces (**c**) and peak change (**d**) in OT1.0 fluorescence; where indicated, DCZ or OT were applied to the slices. n = 7 slices from 2 mice for OT-hM3Dq and n = 5 slices from 2 mice for no-hM3Dq. Two-tailed Student's *t*-tests were performed (p = 8.9×10^{-6} (left) and 0.41 (right)). ***$p < 0.001$ and n.s., not significant. Summary data are presented as the mean±s.e.m.

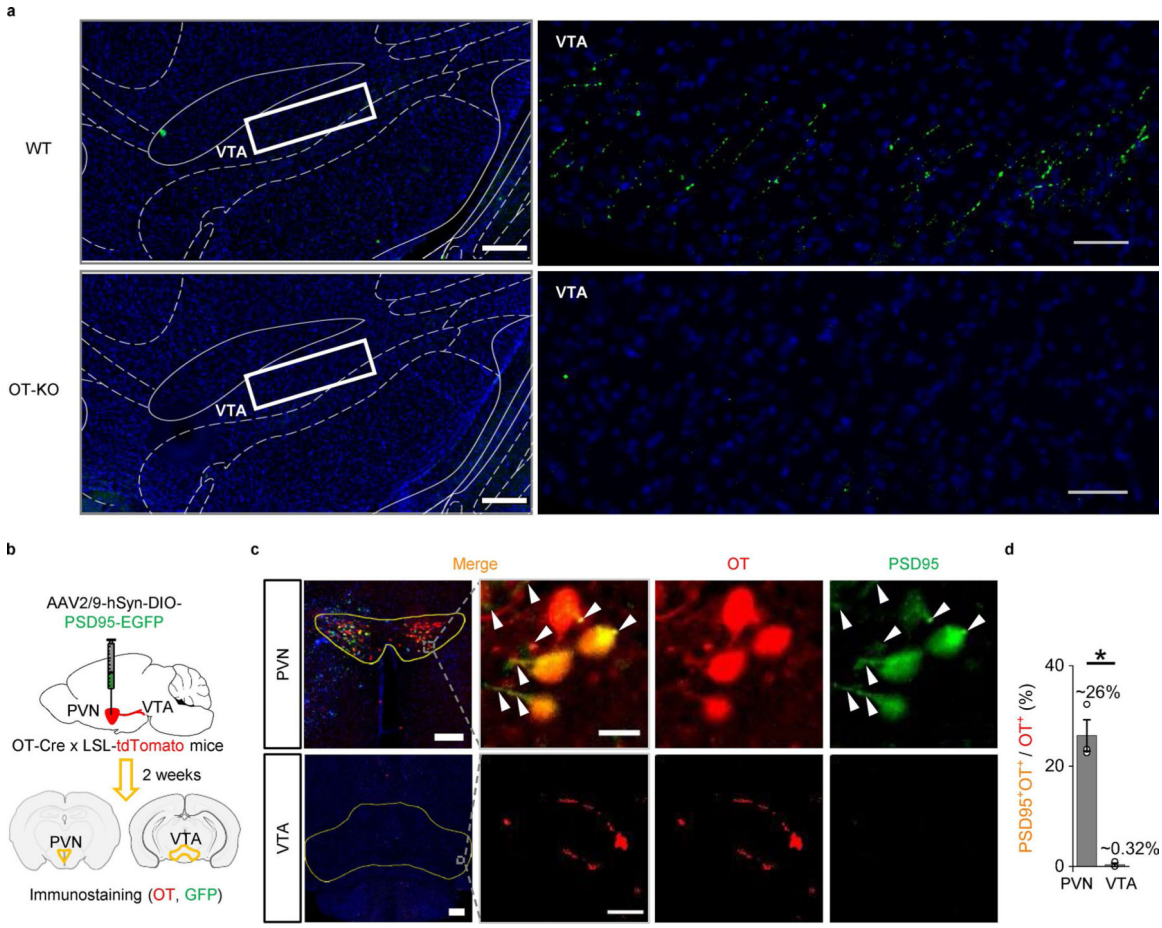

Extended Data Fig. 4 |. Immunostaining of OT neurites in the VTA and PVN.

a. Representative images of OT-positive axons in the VTA of WT and OT-KO mice. Green, OT antibody; blue, DAPI. Scale bars: left, 1 mm; right, 100 μm. **b-d**. Schematic drawings depicting the experimental strategy (**b**), representative images (**c**), and quantification data (**d**) showing the colocalization of PSD95-EGFP with OT-positive neurites in the PVN or VTA of coronal slices. Red, OT (indicated by OT antibody in the VTA or tdTomato in the PVN); green, PSD95 (indicated by GFP antibody); blue, DAPI. $n = 3$ slices from 1 mouse. Two-tailed Student's t-tests were performed ($p = 0.014$). Scale bars: left, 200 μm; right, 20 μm. *p < 0.05. Summary data are presented as the mean±s.e.m.

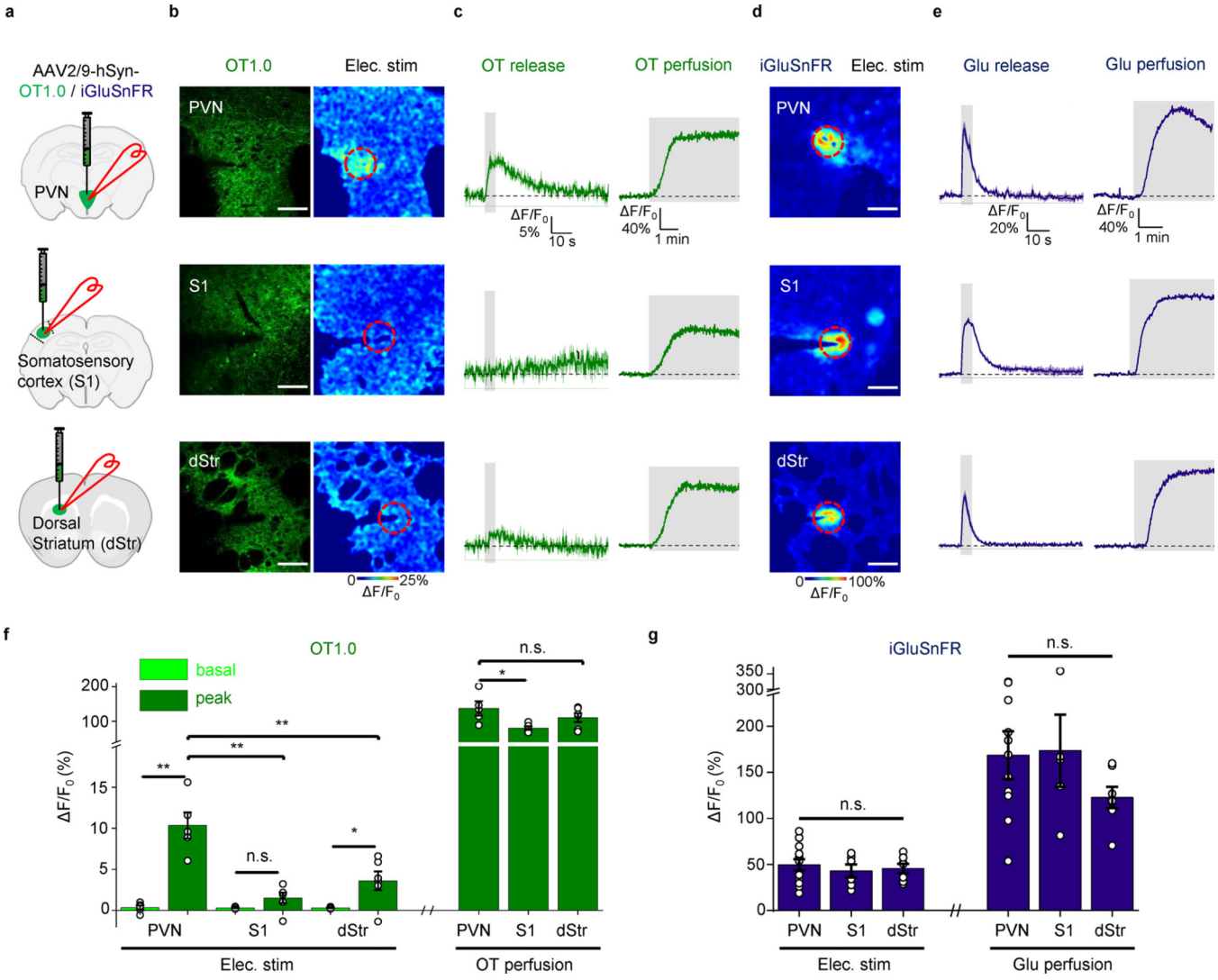

Extended Data Fig. 5 |. Electrical stimulation evoked OT and Glutamate release in the PVN, S1 and dStr.

a. Schematic illustration depicting the experimental setup for panels (**b**-**g**). **b** and **d**. Representative fluorescence images (left) and $\Delta F/F_0$ pseudocolor images (right) showing the expression and electrical stimulation-induced response of OT1.0 or iGluSnFR in the PVN, S1, and dStr. **c** and **e**. Representative traces of electrical stimulation evoked and 100 nM OT or 100 μM Glu perfusion induced OT1.0 or iGluSnFR signals. **f** and **g**. Summary of the change in OT1.0 or iGluSnFR fluorescence in response to 100 pulses or ligand application (n = 5 slices from 4 mice [5/4], 6/3, and 6/3 mice for OT1.0 in the PVN, S1, and dStr, respectively; n = 12 slices from 4 mice [12/4], 6/2, and 7/2 mice for iGluSnFR in the PVN, S1, and dStr, respectively.) Two-tailed Student's t-tests were performed (**f**: for electrical stimulation, $p = 2.9 \times 10^{-3}$, 0.11, and 0.034 between basal and peak $\Delta F/F_0$ for PVN, S1, and dStr, respectively; $p = 3.1 \times 10^{-3}$ between PVN and S1; $p = 9.5 \times 10^{-3}$ between PVN and dStr; for OT perfusion, p = 0.037 between PVN and S1; p = 0.27 between PVN and dStr; **g**: for electrical stimulation, p = 0.50 between PVN and S1; p = 0.63 between PVN and dStr; p = 0.77 between S1 and dStr; for Glu perfusion, p = 0.92 between PVN and S1; p = 0.12

between PVN and dStr; $p = 0.26$ between S1 and dStr). The data of OT1.0 and iGluSnFR in the PVN are reused from Fig. 5. *p < 0.05, **p < 0.01, and n.s., not significant. All scale bars represent 100 μm. Summary data are presented as the mean±s.e.m.

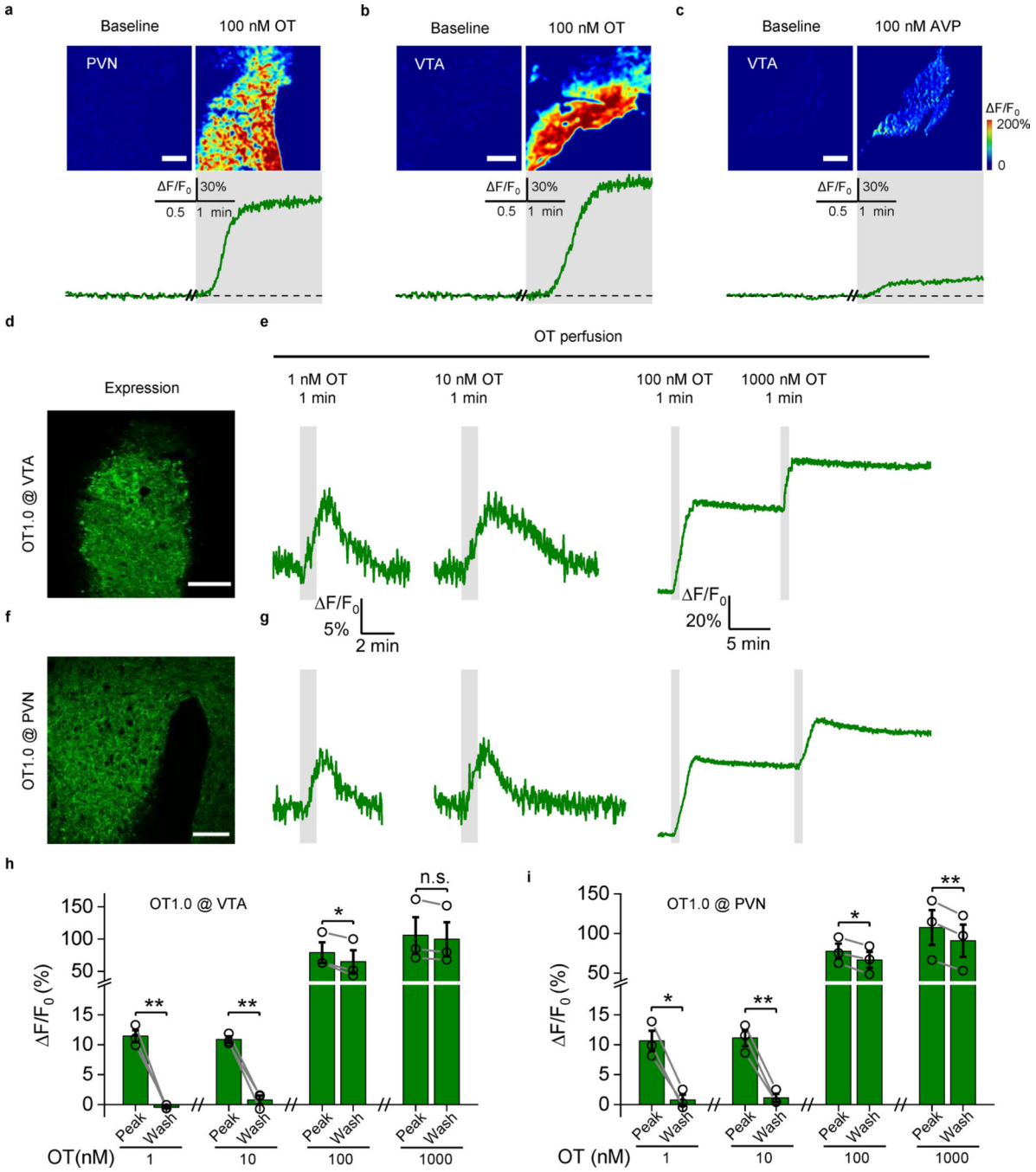

Extended Data Fig. 6 |. Application of OT with different concentrations in OT1.0 expressing slices.

a-c. Example pseudocolor images (top) and fluorescence traces (bottom) of OT1.0-expressing slices containing the PVN (**a**) or VTA (**b, c**) before and after application of 100 nM OT (**a, b**) or AVP (**c**). **d**, **f**. Representative fluorescence images showing the expression

of OT1.0 in the VTA (**d**) and PVN (**f**). **e**, **g**. Example traces of OT1.0 signals in response to 1, 10, 100, and 1000 nM OT application in the VTA (**e**) and PVN (**g**). **h**, **i**. Summary of peak and post-application (wash) $\Delta F/F_0$ in response to 1, 10, 100, and 1000 nM OT in the VTA (**h**) and PVN (**i**). $n = 3$ slices from 3 mice [3/3] and 3/2 mice for OT1.0 in the VTA and PVN, respectively. Two-tailed Student's t-tests were performed (**h**: $p = 0.057$, 0.024, 0.18, and 0.31 (between Peak and Wash) for 1, 10, 100, and 1000 nM OT, respectively; **i**: $p = 0.011$, 8.5×10^{-3}, 0.021, and 9.2×10^{-3} (between Peak and Wash) for 1, 10, 100, and 1000 nM OT, respectively). *p < 0.05, **p < 0.01, and n.s., not significant. All scale bars represent 100 μm. Summary data are presented as the mean±s.e.m.

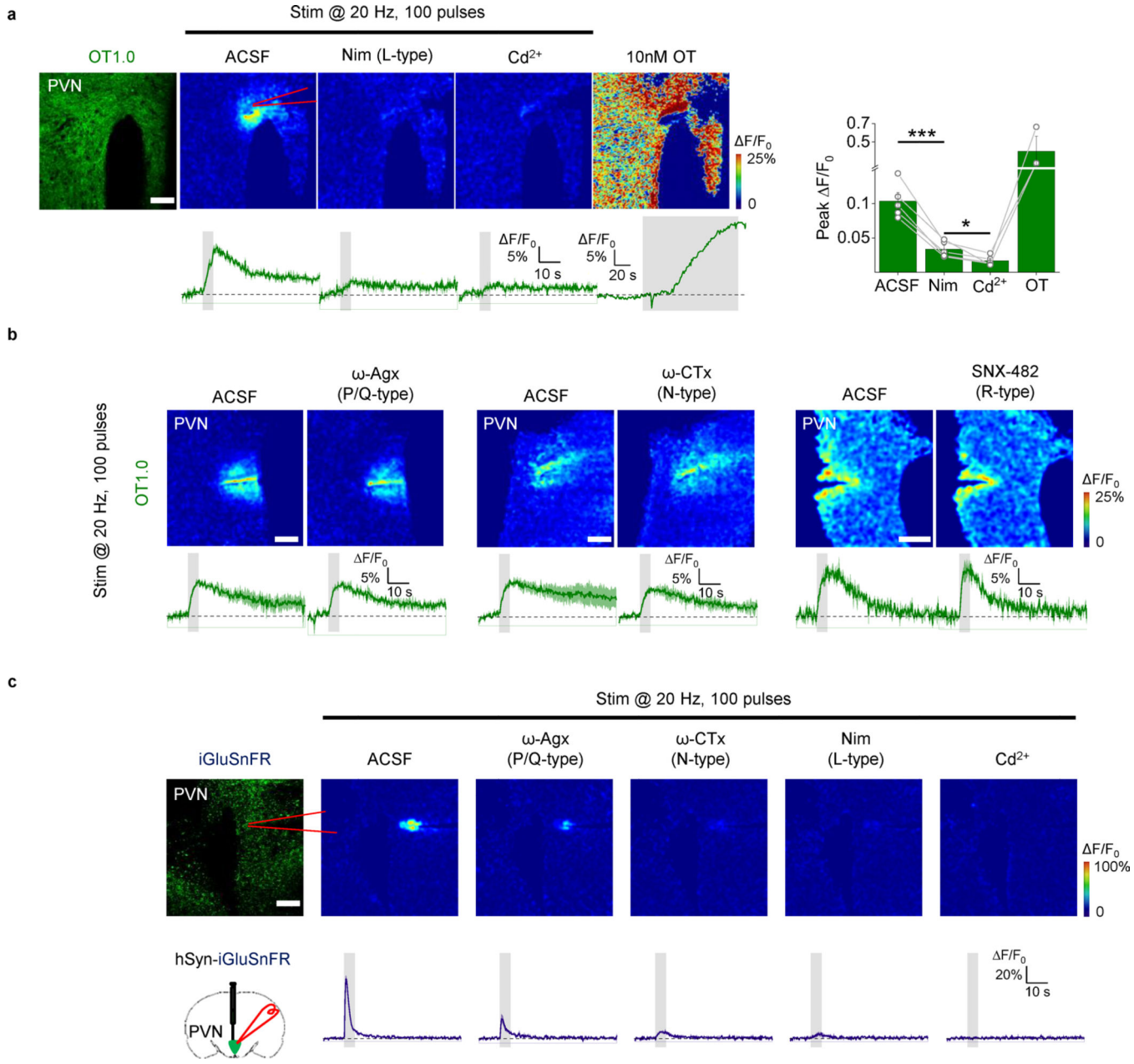

Extended Data Fig. 7 |. Dissecting the Ca^{2+} sources underlying somatodendritic OT release.
a. Top left: representative image of OT1.0 expressed in the PVN (left). Also shown are example pseudocolor images (top row), corresponding traces (bottom row), and summary of the peak OT1.0 response (right) to 100 electrical stimuli delivered at 20 Hz in ACSF, nimodipine (Nim; 10 μM), Cd^{2+} (200 μM), or 10 nM OT. n = 5 slices from 3 mice for ACSF, Nim, and Cd^{2+}; n = 3 slices from 2 mice for OT. Paired two-tailed Student's *t*-tests were performed ($p = 9.7 \times 10^{-4}$ (left) and 0.031 (right)). **b**. Representative pseudocolor images (top row) and corresponding traces (bottom row) of OT1.0 expressed in the PVN in response to 100 electrical stimuli delivered at 20 Hz in ACSF, ω-Agx-IVA (0.3 μM), ω-CTx (1 μM), or SNX-482 (100 nM) to block P/Q-, N-, and R-type VGCCs, respectively. **c**. Representative fluorescence image of iGluSnFR (top left) and schematic drawing depicting the experimental strategy (bottom left), related to Fig. 3e, f. Example pseudocolor images (top) and traces (bottom) of the change in iGluSnFR fluorescence in response to 100 electrical pulses delivered at 20 Hz in ACSF, ω-Agx-IVA (0.3 μM), ω-CTx (1 μM), nimodipine (Nim; 10 μM), or Cd^{2+} (200 μM) to block P/Q-, N-, L-type or all VGCCs, respectively (slices were sequentially perfused with the indicated blockers). *$p < 0.05$ and **$p < 0.01$. All scale bars represent 100 μm. Summary data are presented as the mean±s.e.m.

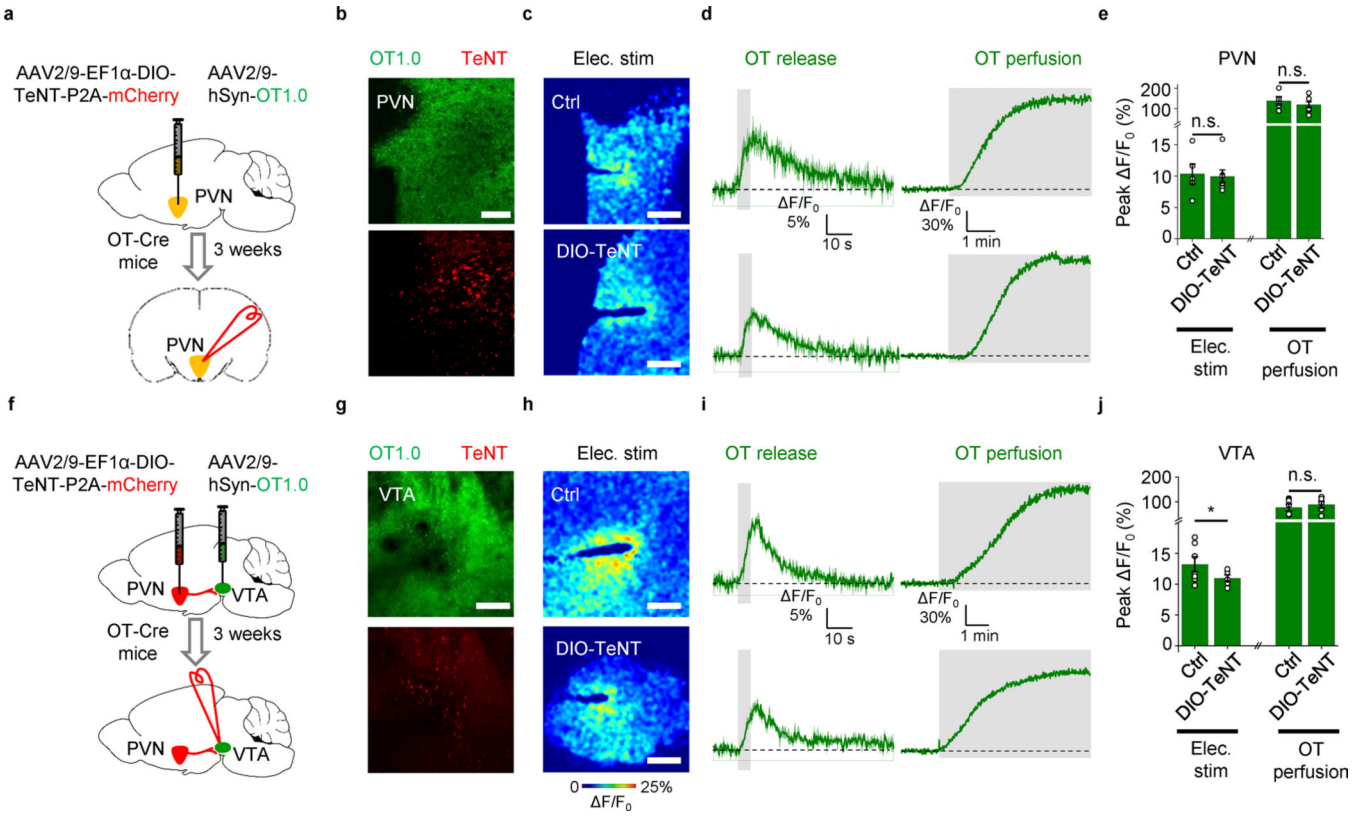

Extended Data Fig. 8 |. Somatodendritic OT release is insensitive to cell type-specific expression of TeNT.
a-j. Schematic drawings depicting the experimental strategy (**a**, **f**), representative images showing the expression (**b**, **g**) and peak response of OT1.0 sensor (**c**, **h**), average traces (**d**, **i**),

and summary (**e**, **j**) of OT1.0 in response to 100 pulses stimulation delivered at 20 Hz or OT perfusion applied under the indicated conditions. $n = 7$ slices from 2 mice [7/2] and 5/2 mice for PVN and VTA, respectively. Two-tailed Student's t-tests were performed (**e**: $p = 0.83$ and 0.47 between Ctrl and DIO-TeNT for electrical stimulation and OT perfusion; **j**: $p = 0.038$ and 0.78 between Ctrl and DIO-TeNT for electrical stimulation and OT perfusion). The data of Ctrl groups in the PVN and VTA are reused from Fig. 5. Scale bars, 100 μm. $*p < 0.05$ and n.s., not significant. Summary data are presented as the mean±s.e.m.

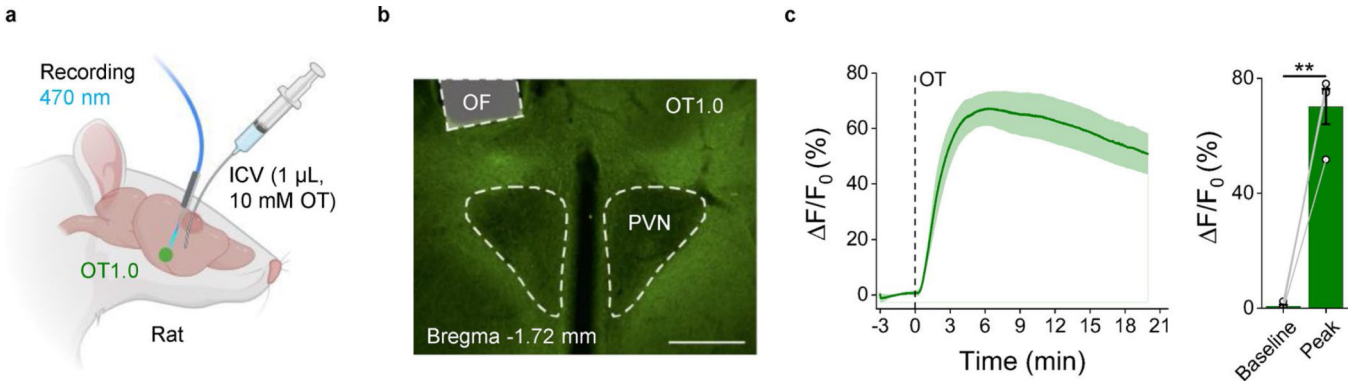

Extended Data Fig. 9 |. OT1.0 can detect intraventricularly injected OT in the PVN of rats.
a. Schematic diagram depicting the experimental strategy for in vivo recording of OT1.0 in rats. An AAV expressing hSyn-OT1.0 was injected into the PVN of WT Sprague Dawley female rats; optical fibers were placed in the above PVN 2 weeks later, 10 mM OT (1 μL) was injected into the lateral ventricle during recording, and 470-nm light was used to excite the OT1.0 sensor together with isosbestic control signal (405 nm). **b**. Exemplary histological verification of the optic fiber placement and the OT1.0 expression in the periPVN area. OT1.0 was stained with anti-GFP antibody for visualization. OF, optic fiber. Scale bar, 400 μm. **c**. Average trace and quantification of OT1.0 signal. The OT1.0 and isosbestic signals were sampled at 1 Hz. n = 4 rats. Paired two-tailed Student's *t*-tests were performed ($p = 1.3 \times 10^{-3}$). $**p < 0.01$. Summary data are presented as the mean±s.e.m.

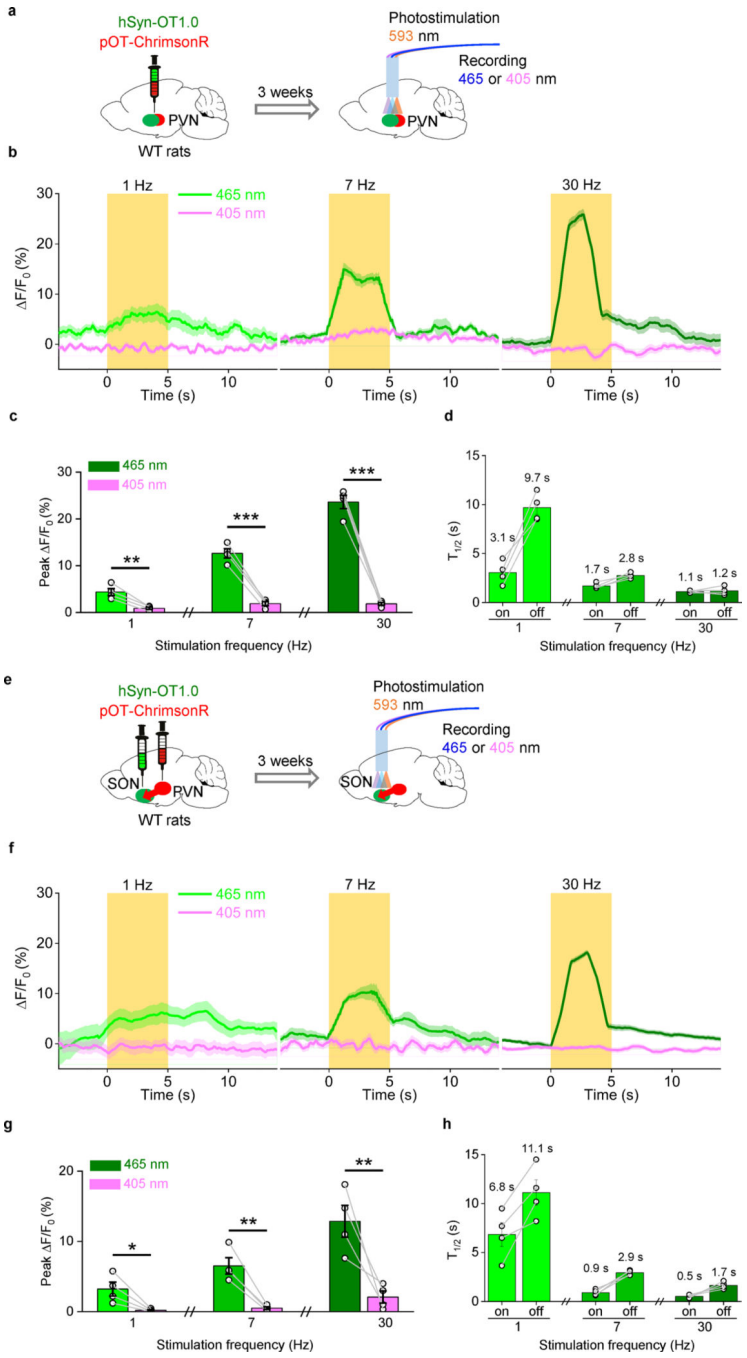

Extended Data Fig. 10 |. Optogenetic activation of neurons induces somatodendritic and axonal OT release in vivo in freely moving rats.

a. Schematic illustrations depicting the optogenetic activation experiments with both the OT sensor and the optogenetic stimulation by ChrimsonR in the PVN. **b**. Representative traces recorded in the rat PVN of changes in normalized fluorescent emission $\Delta F/F_0$ (525 nm) during excitation at isosbestic control (405 nm, in purple) or sensor wavelength (465 nm, in green) before, during and after stimulation of ChrimsonR with pulses (at 593 nm, in orange) of 10 ms at a frequency of 1, 7 or 30 Hz for a total duration of 5 s). **c**. Summary of the

peak changes in OT1.0 fluorescence emission (at 525 nm) during excitation at the sensor wavelength (465 nm, in green) or isosbestic control (405 nm, in purple) in rats PVN (at 1, 7, or 30 Hz photostimulation). n = 4 rats per group. Paired two-tailed Student's *t*-tests were performed between 465 nm and 405 nm ($p = 9.1 \times 10^{-3}$, 6.1×10^{-4}, and 6.6×10^{-4} for 1, 7, and 30 Hz, respectively). **d**. Summary of the rise time ('on') and decay time ('off') constants ($T_{1/2}$) of the OT1.0 response to photostimulation. n = 4 rats per group. **e**. Schematic illustrations depicting the optogenetic activation experiments with OT sensor expressed in the SON and the optogenetic stimulator ChrimsonR expressed in the PVN. **f**. Representative traces recorded in the rat SON of changes in normalized fluorescent emission $\Delta F/F_0$ (525 nm) during excitation at isosbestic control (405 nm, in purple) or sensor wavelength (465 nm, in green) before, during and after stimulation of ChrimsonR (at 593 nm, in orange) with pulses of 10 ms at a frequency of 1, 7, or 30 Hz for a total duration of 5 s). **g**. Summary of the peak change in OT1.0 fluorescence emission (at 525 nm) during excitation at the sensor wavelength (465 nm, in green) or isosbestic control (405 nm, in purple) in rats SON (at 1, 7, or 30 Hz photostimulation). n = 4 rats per group. Paired two-tailed Student's *t*-tests were performed between 465 nm and 405 nm ($p = 0.043$, 8.8×10^{-3}, and 0.034 for 1, 7, and 30 Hz, respectively). **h**. Summary of the rise time ('on') and decay time ('off') constants ($T_{1/2}$) of the OT1.0 response to photostimulation. n = 4 rats per group. $^{*}p < 0.05$, $^{**}p < 0.01$ and $^{***}p < 0.001$. Summary data are presented as the mean±s.e.m.

Supplementary Material

Refer to Web version on PubMed Central for supplementary material.

Acknowledgements

This research was supported by the National Key R&D Program of China (2019YFE011781), the National Natural Science Foundation of China (31925017 and 31871087), the NIH BRAIN Initiative (1U01NS113358 and 1U01NS120824), the Feng Foundation of Biomedical Research, the Clement and Xinxin Foundation, and grants from the Peking-Tsinghua Center for Life Sciences and the State Key Laboratory of Membrane Biology at Peking University School of Life Sciences (to Y.L.); the National Natural Science Foundation of China (81871134) (to P.W.); NIH grants (R01MH101377, R01HD092596, U19NS107616 and U01NS113358), the Mathers Foundation and the Vulnerable Brain Project (to D.L.); the Levy Leon fellowship (to M.L.); the Uehara Memorial Foundation, a JSPS Overseas Research Fellowship and the Osamu Hayaishi Memorial Scholarship (to T.O.); Swiss National Science Foundation grants (CRSK-3_190779, 310030_192463, 310030E_173565) and the Synapsis Foundation (to R.S.); German Research Foundation (DFG) grants (GR 3619/13-1, GR 3619/15-1, GR 3619/16-1) and the SFB Consortium 1158-2 (to V.G.); and the Humboldt Research Fellowship (to A.K.). We thank Y. Rao for sharing the two-photon microscope and X. Lei at PKU-CLS and the National Center for Protein Sciences at Peking University for providing support for the Opera Phenix high-content screening system and imaging platform. We thank L. Barteczko for packaging the viral vectors used for the in vivo experiments of A.K. and V.G. We thank X. Yu at Peking University, B. Li at Cold Spring Harbor Laboratory, D. Anderson at the California Institute of Technology, M. Andermann at Harvard University, P. Kalugin at Harvard University and members of the Li laboratory for helpful suggestions and comments on the manuscript.

Data availability

Plasmids for expressing OT1.0 and OT1.0mut used in this study have been deposited to Addgene (185384-185389; https://www.addgene.org/Yulong_Li/). Source data are provided with this paper.

References

1. Jahr CE & Nicoll RA Dendrodendritic inhibition: demonstration with intracellular recording. Science 207, 1473–1475 (1980). [PubMed: 7361098]
2. Cheramy A, Leviel V. & Glowinski J. Dendritic release of dopamine in the substantia nigra. Nature 289, 537–542 (1981). [PubMed: 6258083]
3. Castel M, Morris J. & Belenky M. Non-synaptic and dendritic exocytosis from dense-cored vesicles in the suprachiasmatic nucleus. Neuroreport 7, 543–547 (1996). [PubMed: 8730825]
4. Simmons ML, Terman GW, Gibbs SM & Chavkin C. L-type calcium channels mediate dynorphin neuropeptide release from dendrites but not axons of hippocampal granule cells. Neuron 14, 1265–1272 (1995). [PubMed: 7605635]
5. Ludwig M. et al. Intracellular calcium stores regulate activity-dependent neuropeptide release from dendrites. Nature 418, 85–89 (2002). [PubMed: 12097911]
6. Ludwig M. & Leng G. Dendritic peptide release and peptide-dependent behaviours. Nat. Rev. Neurosci 7, 126–136 (2006). [PubMed: 16429122]
7. Kennedy MJ & Ehlers MD Mechanisms and function of dendritic exocytosis. Neuron 69, 856–875 (2011). [PubMed: 21382547]
8. Pow DV & Morris JF Dendrites of hypothalamic magnocellular neurons release neurohypophysial peptides by exocytosis. Neuroscience 32, 435–439 (1989). [PubMed: 2586758]
9. Ludwig M. Dendritic release of vasopressin and oxytocin. J. Neuroendocrinol 10, 881–895 (1998). [PubMed: 9870745]
10. Rhodes CH, Morrell JI & Pfaff DW Immunohistochemical analysis of magnocellular elements in rat hypothalamus: distribution and numbers of cells containing neurophysin, oxytocin, and vasopressin. J. Comp. Neurol 198, 45–64 (1981). [PubMed: 7014660]
11. Gimpl G. & Fahrenholz F. The oxytocin receptor system: structure, function, and regulation. Physiol. Rev 81, 629–683 (2001). [PubMed: 11274341]
12. Cunningham ET Jr. & Sawchenko PE Reflex control of magnocellular vasopressin and oxytocin secretion. Trends Neurosci. 14, 406–411 (1991). [PubMed: 1720582]
13. Jurek B. & Neumann ID The oxytocin receptor: from intracellular signaling to behavior. Physiol. Rev 98, 1805–1908 (2018). [PubMed: 29897293]
14. Ludwig M. & Pittman QJ Talking back: dendritic neurotransmitter release. Trends Neurosci. 26, 255–261 (2003). [PubMed: 12744842]
15. Ferguson JN et al. Social amnesia in mice lacking the oxytocin gene. Nat. Genet 25, 284–288 (2000). [PubMed: 10888874]
16. Andari E. et al. Promoting social behavior with oxytocin in high-functioning autism spectrum disorders. Proc. Natl Acad. Sci. USA 107, 4389–4394 (2010). [PubMed: 20160081]
17. Nishioka T, Anselmo-Franci JA, Li P, Callahan MF & Morris M. Stress increases oxytocin release within the hypothalamic paraventricular nucleus. Brain Res. 781, 57–61 (1998). [PubMed: 9507065]
18. Rosenfeld AJ., Lieberman JA. & Jarskog LF. Oxytocin, dopamine, and the amygdala: a neurofunctional model of social cognitive deficits in schizophrenia. Schizophr. Bull 37, 1077–1087 (2011). [PubMed: 20308198]
19. Bito L, Davson H, Levin E, Murray M. & Snider N. The concentrations of free amino acids and other electrolytes in cerebrospinal fluid, in vivo dialysate of brain, and blood plasma of the dog. J. Neurochem 13, 1057–1067 (1966). [PubMed: 5924657]
20. Robinson IC & Jones PM Oxytocin and neurophysin in plasma and CSF during suckling in the guinea-pig. Neuroendocrinology 34, 59–63 (1982). [PubMed: 7057961]
21. Neumann I, Russell JA & Landgraf R. Oxytocin and vasopressin release within the supraoptic and paraventricular nuclei of pregnant, parturient and lactating rats: a microdialysis study. Neuroscience 53, 65–75 (1993). [PubMed: 8469313]
22. Pinol RA, Jameson H, Popratiloff A, Lee NH & Mendelowitz D. Visualization of oxytocin release that mediates paired pulse facilitation in hypothalamic pathways to brainstem autonomic neurons. PLoS ONE 9, e112138 (2014).

23. Mignocchi N, Krüssel S, Jung K, Lee D. & Kwon H-B Development of a genetically-encoded oxytocin sensor. Preprint at bioRxiv 10.1101/2020.07.14.202598 (2020).
24. Ino D, Tanaka Y, Hibino H. & Nishiyama M. A fluorescent sensor for real-time measurement of extracellular oxytocin dynamics in the brain. Nat Methods 19, 1286–1294 (2022). [PubMed: 36138174]
25. Jing M. et al. A genetically encoded fluorescent acetylcholine indicator for in vitro and in vivo studies. Nat. Biotechnol 36, 726–737 (2018). [PubMed: 29985477]
26. Patriarchi T. et al. Ultrafast neuronal imaging of dopamine dynamics with designed genetically encoded sensors. Science 360, eaat4422 (2018).
27. Sun F. et al. A genetically encoded fluorescent sensor enables rapid and specific detection of dopamine in flies, fish, and mice. Cell 174, 481–496 (2018). [PubMed: 30007419]
28. Feng J. et al. A genetically encoded fluorescent sensor for rapid and specific in vivo detection of norepinephrine. Neuron 102, 745–761 (2019). [PubMed: 30922875]
29. Jing M. et al. An optimized acetylcholine sensor for monitoring in vivo cholinergic activity. Nat. Methods 17, 1139–1146 (2020). [PubMed: 32989318]
30. Patriarchi T. et al. An expanded palette of dopamine sensors for multiplex imaging in vivo. Nat. Methods 17, 1147–1155 (2020). [PubMed: 32895537]
31. Peng W. et al. Regulation of sleep homeostasis mediator adenosine by basal forebrain glutamatergic neurons. Science 369, eabb0556 (2020).
32. Sun F. et al. Next-generation GRAB sensors for monitoring dopaminergic activity in vivo. Nat. Methods 17, 1156–1166 (2020). [PubMed: 33087905]
33. Dong A. et al. A fluorescent sensor for spatiotemporally resolved imaging of endocannabinoid dynamics in vivo. Nat. Biotechnol 40, 787–798 (2022). [PubMed: 34764491]
34. Wan J. et al. A genetically encoded sensor for measuring serotonin dynamics. Nat. Neurosci 24, 746–752 (2021). [PubMed: 33821000]
35. Wu Z. et al. A sensitive GRAB sensor for detecting extracellular ATP in vitro and in vivo. Neuron 110, 770–782 (2022). [PubMed: 34942116]
36. Kroeze WK et al. PRESTO-Tango as an open-source resource for interrogation of the druggable human GPCRome. Nat. Struct. Mol. Biol 22, 362–369 (2015). [PubMed: 25895059]
37. Busnelli M. et al. Functional selective oxytocin-derived agonists discriminate between individual G protein family subtypes. J. Biol. Chem 287, 3617–3629 (2012). [PubMed: 22069312]
38. Nagai Y. et al. Deschloroclozapine, a potent and selective chemogenetic actuator enables rapid neuronal and behavioral modulations in mice and monkeys. Nat. Neurosci 23, 1157–1167 (2020). [PubMed: 32632286]
39. Beier KT et al. Circuit architecture of VTA dopamine neurons revealed by systematic input–output mapping. Cell 162, 622–634 (2015). [PubMed: 26232228]
40. Hung LW et al. Gating of social reward by oxytocin in the ventral tegmental area. Science 357, 1406–1411 (2017). [PubMed: 28963257]
41. Xiao L., Priest MF., Nasenbeny J., Lu T. & Kozorovitskiy Y. Biased oxytocinergic modulation of midbrain dopamine systems. Neuron 95, 368–384 (2017). [PubMed: 28669546]
42. Barg S. et al. Delay between fusion pore opening and peptide release from large dense-core vesicles in neuroendocrine cells. Neuron 33, 287–299 (2002). [PubMed: 11804575]
43. Marvin JS et al. Stability, affinity, and chromatic variants of the glutamate sensor iGluSnFR. Nat. Methods 15, 936–939 (2018). [PubMed: 30377363]
44. van den Pol AN Neuropeptide transmission in brain circuits. Neuron 76, 98–115 (2012). [PubMed: 23040809]
45. Lewis EM et al. Parallel social information processing circuits are differentially impacted in autism. Neuron 108, 659–675 (2020). [PubMed: 33113347]
46. Fisher TE & Bourque CW Calcium-channel subtypes in the somata and axon terminals of magnocellular neurosecretory cells. Trends Neurosci. 19, 440–444 (1996). [PubMed: 8888522]
47. Xu S. et al. Behavioral state coding by molecularly defined paraventricular hypothalamic cell type ensembles. Science 370, eabb2494 (2020).

48. Romanov RA et al. Molecular interrogation of hypothalamic organization reveals distinct dopamine neuronal subtypes. Nat. Neurosci 20, 176–188 (2017). [PubMed: 27991900]
49. Tobin VA, Douglas AJ, Leng G. & Ludwig M. The involvement of voltage-operated calcium channels in somato-dendritic oxytocin release. PLoS ONE 6, e25366 (2011). [PubMed: 22028774]
50. Wheeler DB, Randall A. & Tsien RW Roles of N-type and Q-type Ca^{2+} channels in supporting hippocampal synaptic transmission. Science 264, 107–111 (1994). [PubMed: 7832825]
51. Hirasawa M, Kombian SB & Pittman QJ Oxytocin retrogradely inhibits evoked, but not miniature, EPSCs in the rat supraoptic nucleus: role of N- and P/Q-type calcium channels. J. Physiol 532, 595–607 (2001). [PubMed: 11313432]
52. Sudhof TC & Rothman JE Membrane fusion: grappling with SNARE and SM proteins. Science 323, 474–477 (2009). [PubMed: 19164740]
53. Kasai H, Takahashi N. & Tokumaru H. Distinct initial SNARE configurations underlying the diversity of exocytosis. Physiol. Rev92, 1915–1964 (2012). [PubMed: 23073634]
54. Schiavo G. et al. Tetanus and botulinum-B neurotoxins block neurotransmitter release by proteolytic cleavage of synaptobrevin. Nature 359, 832–835 (1992). [PubMed: 1331807]
55. Blasi J. et al. Botulinum neurotoxin A selectively cleaves the synaptic protein SNAP-25. Nature 365, 160–163 (1993). [PubMed: 8103915]
56. Bennett MK, Calakos N. & Scheller RH Syntaxin: a synaptic protein implicated in docking of synaptic vesicles at presynaptic active zones. Science 257, 255–259 (1992). [PubMed: 1321498]
57. Yamasaki S. et al. Cleavage of members of the synaptobrevin/ VAMP family by types D and F botulinal neurotoxins and tetanus toxin. J. Biol. Chem 269, 12764–12772 (1994). [PubMed: 8175689]
58. Klapoetke NC et al. Independent optical excitation of distinct neural populations. Nat. Methods 11, 338–346 (2014). [PubMed: 24509633]
59. Oti T. et al. Oxytocin influences male sexual activity via non-synaptic axonal release in the spinal cord. Curr. Biol 31, 103–114 (2021). [PubMed: 33125871]
60. Hillegaart V, Alster P, Uvnas-Moberg K. & Ahlenius S. Sexual motivation promotes oxytocin secretion in male rats. Peptides 19, 39–45 (1998). [PubMed: 9437735]
61. Hughes AM, Everitt BJ, Lightman SL & Todd K. Oxytocin in the central nervous system and sexual behaviour in male rats. Brain Res. 414, 133–137 (1987). [PubMed: 3620914]
62. Witt DM & Insel TR Increased Fos expression in oxytocin neurons following masculine sexual behavior. J. Neuroendocrinol 6, 13–18 (1994). [PubMed: 8025564]
63. Argiolas A. & Melis MR. The role of oxytocin and the paraventricular nucleus in the sexual behaviour of male mammals. Physiol. Behav 83, 309–317 (2004). [PubMed: 15488547]
64. Clement P. et al. Brain oxytocin receptors mediate ejaculation elicited by 7-hydroxy-2-(di-N-propylamino) tetralin (7-OH-DPAT) in anaesthetized rats. Br. J. Pharmacol 154, 1150–1159 (2008). [PubMed: 18469843]
65. Gil M, Bhatt R, Picotte KB & Hull EM Oxytocin in the medial preoptic area facilitates male sexual behavior in the rat. Horm. Behav 59, 435–443 (2011). [PubMed: 21195714]
66. Yu P, Zhang M, Nan X, Zhao H. & Gong D. Differences in the number of oxytocin, vasopressin, and tyrosine hydroxylase cells in brain regions associated with mating among great, midday, and Mongolian gerbils. Brain Res. 1733, 146677 (2020). [PubMed: 32001244]
67. Melis MR et al. Oxytocin injected into the ventral tegmental area induces penile erection and increases extracellular dopamine in the nucleus accumbens and paraventricular nucleus of the hypothalamus of male rats. Eur. J. Neurosci 26, 1026–1035 (2007). [PubMed: 17672853]
68. Argiolas A. & Melis MR Central control of penile erection: role of the paraventricular nucleus of the hypothalamus. Prog. Neurobiol 76, 1–21 (2005). [PubMed: 16043278]
69. Miesenbock G, De Angelis DA & Rothman JE Visualizing secretion and synaptic transmission with pH-sensitive green fluorescent proteins. Nature 394, 192–195 (1998). [PubMed: 9671304]
70. Ludwig M. et al. Regulation of activity-dependent dendritic vasopressin release from rat supraoptic neurones. J. Physiol 564, 515–522 (2005). [PubMed: 15731188]
71. Neumann ID & Landgraf R. Balance of brain oxytocin and vasopressin: implications for anxiety, depression, and social behaviors. Trends Neurosci. 35, 649–659 (2012). [PubMed: 22974560]

72. Busnelli M, Bulgheroni E, Manning M, Kleinau G. & Chini B. Selective and potent agonists and antagonists for investigating the role of mouse oxytocin receptors. J. Pharmacol. Exp. Ther346, 318–327 (2013). [PubMed: 23723434]
73. Manning M. et al. Oxytocin and vasopressin agonists and antagonists as research tools and potential therapeutics. J. Neuroendocrinol 24, 609–628 (2012). [PubMed: 22375852]
74. Postina R, Kojro E. & Fahrenholz F. Separate agonist and peptide antagonist binding sites of the oxytocin receptor defined by their transfer into the V2 vasopressin receptor. J. Biol. Chem 271, 31593–31601 (1996). [PubMed: 8940177]
75. Kimura T. et al. Molecular characterization of a cloned human oxytocin receptor. Eur. J. Endocrinol 131, 385–390 (1994). [PubMed: 7921228]
76. Freund-Mercier MJ, Stoeckel ME & Klein MJ Oxytocin receptors on oxytocin neurones: histoautoradiographic detection in the lactating rat. J. Physiol 480, 155–161 (1994). [PubMed: 7853219]
77. Moos F. et al. Release of oxytocin and vasopressin by magnocellular nuclei in vitro: specific facilitatory effect of oxytocin on its own release. J. Endocrinol 102, 63–72 (1984). [PubMed: 6539805]
78. Brown CH, Ludwig M, Tasker JG & Stern JE Somato-dendritic vasopressin and oxytocin secretion in endocrine and autonomic regulation. J. Neuroendocrinol 32, e12856 (2020). [PubMed: 32406599]
79. Chen R, Wu X, Jiang L. & Zhang Y. Single-cell RNA-seq reveals hypothalamic cell diversity. Cell Rep. 18, 3227–3241 (2017). [PubMed: 28355573]
80. Tobin V. et al. Expression of exocytosis proteins in rat supraoptic nucleus neurones. J. Neuroendocrinol 24, 629–641 (2012). [PubMed: 21988098]
81. Jourdain P, Poulain DA, Theodosis DT & Israel JM Electrical properties of oxytocin neurons in organotypic cultures from postnatal rat hypothalamus. J. Neurophysiol 76, 2772–2785 (1996). [PubMed: 8899644]
82. Wang G, Dayanithi G, Newcomb R. & Lemos JR An R-type Ca^{2+} current in neurohypophysial terminals preferentially regulates oxytocin secretion. J. Neurosci 19, 9235–9241 (1999). [PubMed: 10531427]
83. Waldherr M. & Neumann ID Centrally released oxytocin mediates mating-induced anxiolysis in male rats. Proc. Natl Acad. Sci. USA 104, 16681–16684 (2007). [PubMed: 17925443]
84. de Kock CP. et al. . Somatodendritic secretion in oxytocin neurons is upregulated during the female reproductive cycle. J. Neurosci 23, 2726–2734 (2003). [PubMed: 12684458]
85. Althammer F. & Grinevich V. Diversity of oxytocin neurons: beyond magno- and parvocellular cell types? J. Neuroendocrinol 10.1111/jne.12549 (2017).
86. Luther JA & Tasker JG Voltage-gated currents distinguish parvocellular from magnocellular neurones in the rat hypothalamic paraventricular nucleus. J. Physiol 523, 193–209 (2000). [PubMed: 10673555]
87. Zhang B. et al. Reconstruction of the hypothalamo-neurohypophysial system and functional dissection of magnocellular oxytocin neurons in the brain. Neuron 109, 331–346 (2020). [PubMed: 33212012]
88. Swanson LW & Sawchenko PE Hypothalamic integration: organization of the paraventricular and supraoptic nuclei. Annu. Rev. Neurosci 6, 269–324 (1983). [PubMed: 6132586]
89. Eliava M. et al. A new population of parvocellular oxytocin neurons controlling magnocellular neuron activity and inflammatory pain processing. Neuron 89, 1291–1304 (2016). [PubMed: 26948889]
90. Shimojo M. et al. SNAREs controlling vesicular release of BDNF and development of callosal axons. Cell Rep. 11, 1054–1066 (2015). [PubMed: 25959820]
91. Leng G. & Ludwig M. Intranasal oxytocin: myths and delusions. Biol. Psychiatry 79, 243–250 (2016). [PubMed: 26049207]
92. Lee HJ, Macbeth AH, Pagani JH & Young WS 3rd Oxytocin: the great facilitator of life. Prog. Neurobiol 88, 127–151 (2009). [PubMed: 19482229]
93. Bartz JA, Zaki J, Bolger N. & Ochsner KN Social effects of oxytocin in humans: context and person matter. Trends Cogn. Sci15, 301–309 (2011). [PubMed: 21696997]

94. Guastella AJ & Hickie IB Oxytocin treatment, circuitry, and autism: a critical review of the literature placing oxytocin into the autism context. Biol. Psychiatry 79, 234–242 (2016). [PubMed: 26257243]

95. Meyer-Lindenberg A, Domes G, Kirsch P. & Heinrichs M. Oxytocin and vasopressin in the human brain: social neuropeptides for translational medicine. Nat. Rev. Neurosci 12, 524–538 (2011). [PubMed: 21852800]

96. Falkner AL, Grosenick L, Davidson TJ, Deisseroth K. & Lin D. Hypothalamic control of male aggression-seeking behavior. Nat. Neurosci 19, 596–604 (2016). [PubMed: 26950005]

97. Tang Y. et al. Viral vectors for opto-electrode recording and photometry-based imaging of oxytocin neurons in anesthetized and socially interacting rats. STAR Protoc. 3, 101032 (2022). [PubMed: 34977678]

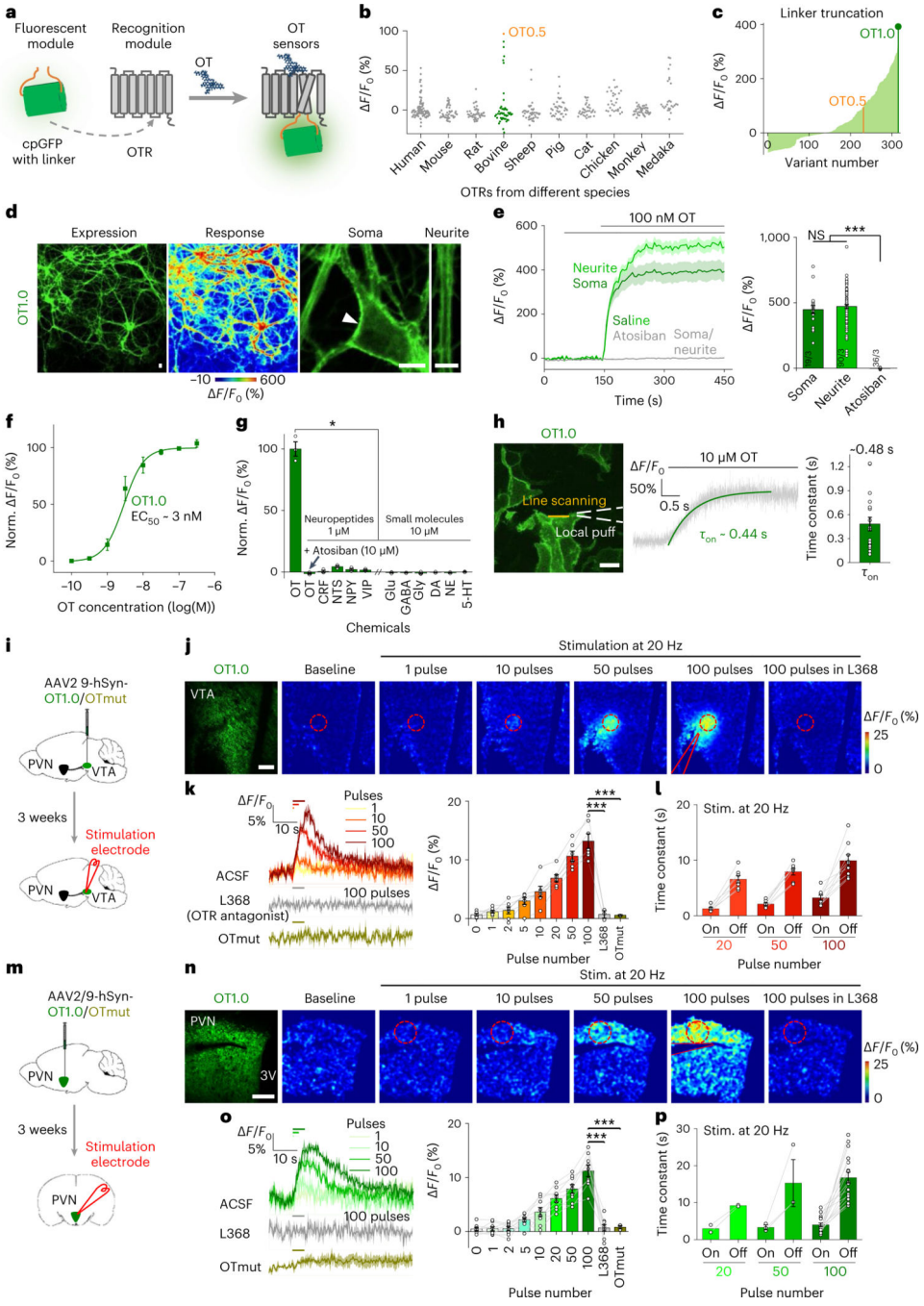

Fig. 1 |. Development of GRAB$_{OT}$ sensors and activity-dependent OT release in brain slices.
a, Schematic diagram depicting the principle behind the GRAB$_{OT}$ sensor. **b**, Selection of a candidate sensor for further development in HEK293T cells by screening OTRs cloned from the indicated species. **c**, Linker length optimization of GRAB$_{OT}$ sensors based on OT0.5. **d**, Left, representative images of OT1.0 expression and the response to 100 nM OT in cultured neurons. Right, representative soma (indicated by the white arrowhead) and neurite images. **e**, Example traces (left) and summary data (right) of OT1.0-expressing neurons pretreated with saline or 10 μM atosiban in response to OT. Soma, n = 19 regions

of interest (ROIs) from 3 dishes (19/3); neurite, $n = 90/3$; atosiban, $n = 36/3$. Two-tailed Student's t tests: $P = 0.50$ (between soma and neurite), $P = 2.3 \times 10^{-18}$ (between soma and atosiban), $P = 7.6 \times 10^{-51}$ (between neurite and atosiban). **f**, Normalized dose–response curve of OT1.0-expressing neurons in response to the indicated concentrations of OT; $n = 4$ dishes. **g**, Summary of normalized $\Delta F/F_0$ measured in OT1.0-expressing neurons in response to the indicated compounds. CRF, corticotropin-releasing factor; NTS, neurotensin; NPY, neuropeptide Y; VIP, vasoactive intestinal peptide; Glu, glutamate; Gly, glycine; DA, dopamine; NE, norepinephrine; 5-HT, 5-hydroxytryptamine. $n = 3$ wells per group. One-way ANOVA: $F(11, 4.446) = 69$, $P = 2.0 \times 10^{-4}$; Dunnett's T3 multiple-comparisons tests, $P =$ 0.030, 0.018, 0.022, 0.020, 0.016, 0.029, 0.030, 0.029, 0.029, 0.029 and 0.029 (from left to right, between OT and other groups, respectively). **h**, Summary of the kinetics of the OT1.0 response: illustration of the local puff system (left), representative response trace (middle) and group data for τ_{on} (right); $n = 18$ cells from 3 cultures. **i**, Schematic illustration depicting the experimental design in the VTA for **j**–**l**. **j**, Example fluorescence and pseudocolor images of OT1.0- or OTmut-expressing brain slices at baseline and in response to the indicated stimuli in the presence of artificial cerebrospinal fluid (ACSF) or 5 μM L368. The dashed red circles indicate the ROI used to calculate the response, and the approximate location of the stimulating electrode is indicated. **k**, Representative traces (left) and summary data (right) for the change in OT1.0 or OTmut fluorescence in response to the indicated stimuli in ACSF or L368. $n = 7$ slices from 5 mice (7/5), 3/2 and 3/1 for ACSF, L368 and OTmut, respectively. Two-tailed Student's t tests: $P = 1.2 \times 10^{-5}$ (between ACSF and L368), $P =$ 3.2×10^{-5} (between ACSF and OTmut). **l**, Summary of the rise and decay time constants (τ_{on} and τ_{off}) of the electrically evoked fluorescence increase in OT1.0-expressing slices in response to the indicated stimuli. $n = 7$, 7 and 9 slices for the 20-, 50- and 100-pulse groups, respectively. **m**, Schematic illustration depicting the experimental design in the PVN for **n**–**p**. **n**–**p**, Similar to **j**–**l**. In **o**, $n = 9$ slices from 5 mice (9/5), 9/5 and 3/1 for ACSF, L368 and OTmut, respectively; in **p**, $n = 2$, 3 and 17 slices for the 20-, 50- and 100-pulse groups, respectively. Paired two-tailed Student's t test, $P = 3.7 \times 10^{-5}$ (between ACSF and L368); two-tailed Student's t test, $P = 3.8 \times 10^{-6}$ (between ACSF and OTmut). $^*P < 0.05$, $^{***}P <$ 0.001; NS, not significant. Scale bars: 10 μm (**d**), 25 μm (**h**) and 100 μm (**j**,**n**). Summary data are presented as the mean ± s.e.m.

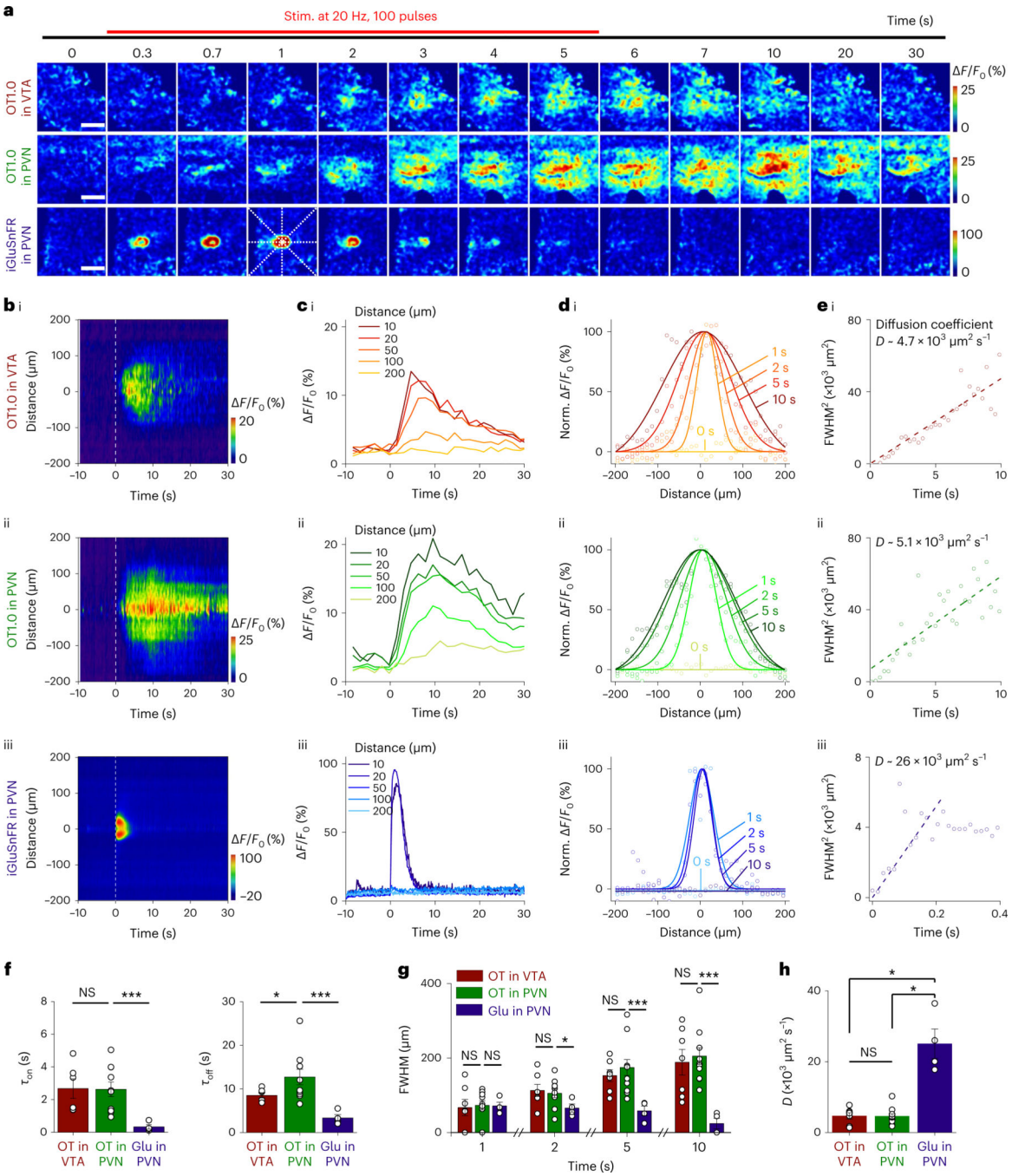

Fig. 2 |. Probing the spatial and temporal dynamics of OT release in the axonal and somatodendritic compartments.

a, Example time-lapse pseudocolor images of OT1.0 expressed in the VTA and PVN and of iGluSnFR expressed in the PVN in acute brain slices. The dashed lines were used to analyze spatial and temporal dynamics. Similar results were observed for more than six slices for each group. Scale bars, 100 μm. **b**, Spatial profile of the evoked change in fluorescence shown in **a**. Each heatmap shows the average of three trials conducted in one slice. **c**, Temporal dynamics of the data shown in **b** measured at the indicated distance from the

release center. The data were processed with 5× binning. **d**, Spatial dynamics of the data shown in **b** measured 1, 2, 5 and 10 s after the start of stimulation. Each curve was fitted with a Gaussian function. The data were processed with 5× binning and normalized to the peak response of each curve. **e**, Representative diffusion coefficients (D) were determined by plotting the square of FWHM (full width at half maximum) against time on the basis of the data shown in **d**. The diffusion coefficients were obtained by fitting a linear function using the $FWHM^2$ calculated from the first 10 s ((i) and (ii)) or the first 0.2 s (iii). In **b**–**e**, data shown are for OT1.0 in the VTA (i) and PVN (ii) and for iGluSnFR in the PVN (iii). **f**, Summary of τ_{on} and τ_{off} for the evoked OT1.0 response in the VTA and PVN and for the iGluSnFR response in the PVN at a distance of 10 μm from the release center (n = 6, 10 and 4 slices, respectively). Two-tailed Student's t tests: τ_{on}: P = 0.95 (between OT in the VTA and OT in the PVN), 5.4×10^{-4} (between OT in the PVN and glutamate in the PVN); τ_{off}: P = 0.046 (between OT in the VTA and OT in the PVN), 4.6×10^{-4} (between OT in the PVN and glutamate in the PVN). **g**, Summary of the FWHM of activity-dependent OT and glutamate signals measured in **d** at the indicated time points; n = 7 slices from 4 mice (7/4), 11/5 and 4/1 for OT in the VTA, OT in the PVN and glutamate in the PVN, respectively. Two-tailed Student's t tests were performed for 1, 2, 5 and 10 s (P = 0.82, 0.70, 0.42 and 0.70 (between OT in the VTA and OT in the PVN); P = 0.93, 0.031, 4.5×10^{-4} and 1.2×10^{-5} (between OT in the PVN and glutamate in the PVN)). **h**, Summary of the diffusion coefficients measured in **e**; n = 7 slices from 4 mice (7/4), 11/5 and 4/1 for OT in the VTA, OT in the PVN and glutamate in the PVN, respectively. Two-tailed Student's t tests: P = 0.93 (between OT in the VTA and OT in the PVN), 0.015 (between OT in the PVN and glutamate in the PVN), 0.014 (between OT in the VTA and glutamate in the PVN). The data for OT in the VTA and OT in the PVN were reanalyzed from raw images used in Fig. 1k,o. *P < 0.05, ***P < 0.001; NS, not significant. Summary data are presented as the mean ± s.e.m.

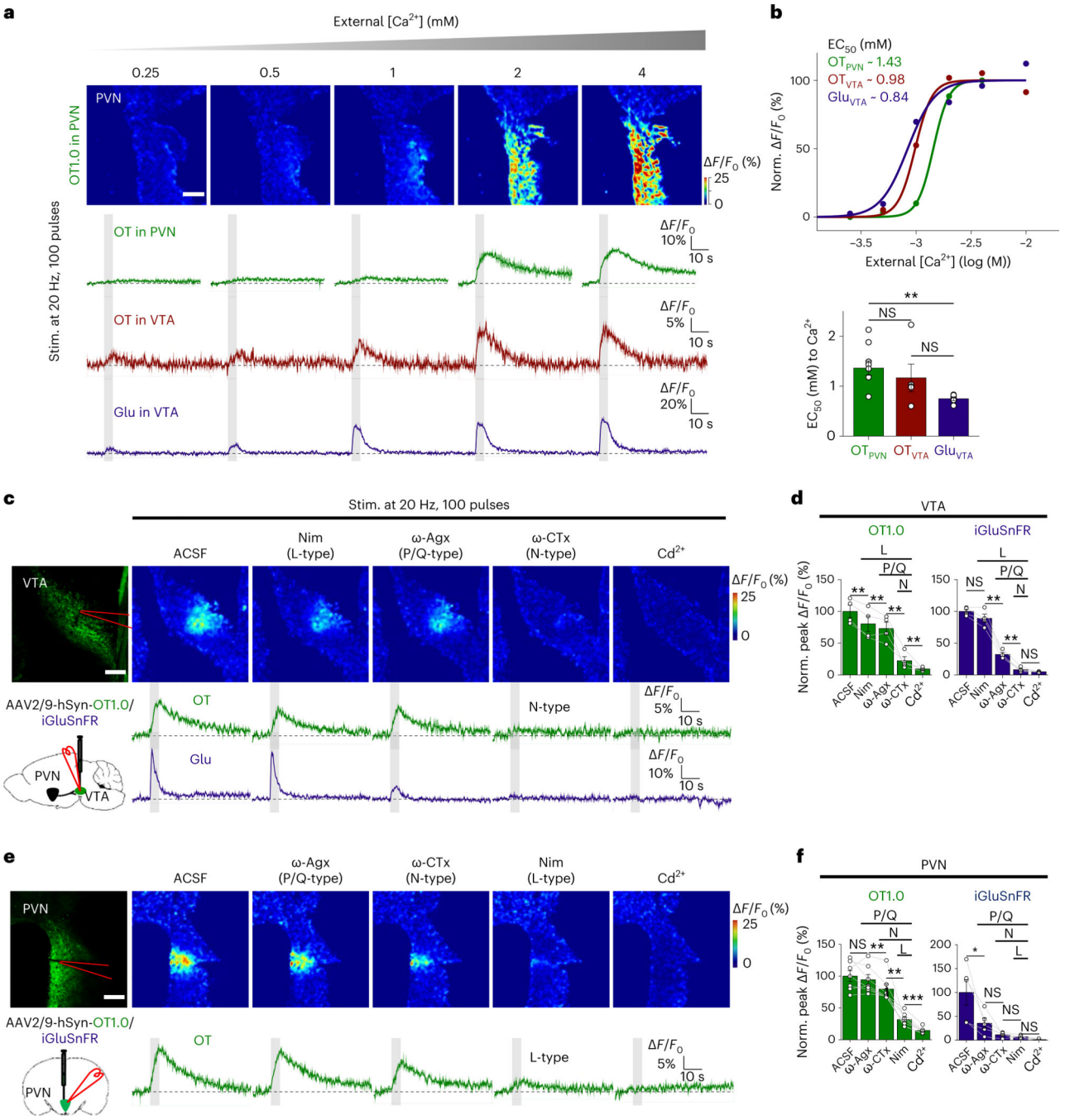

Fig. 3 |. N-type and L-type VGCCs support axonal and somatodendritic OT release, respectively.

a, Pseudocolor two-photon images of evoked OT release in the PVN (top) and average $\Delta F/F_0$ traces of OT1.0 in the PVN, OT1.0 in the VTA and iGluSnFR in the VTA (bottom) in the indicated concentrations of extracellular Ca^{2+}. **b**, Summary of the normalized peak $\Delta F/F_0$ measured in **a** at the indicated Ca^{2+} concentrations (top) and summary of EC_{50} for OT1.0 in the PVN and VTA and iGluSnFR in the VTA (bottom); the data in the upper panel were normalized to the peak response measured in 4 mM Ca^{2+}. $n = 9$ slices from 4 mice (9/4), 5/3 and 5/2 for OT in the PVN, OT in the VTA and glutamate in the VTA,

respectively. Two-tailed Student's *t* tests: $P = 0.55$ (between OT in the PVN and OT in the VTA), $P = 0.21$ (between OT in the VTA and glutamate in the VTA), $P = 2.6 \times 10^{-3}$ (between OT in the PVN and glutamate in the VTA). **c**, Representative fluorescence image of OT1.0 (top left) and schematic drawing depicting the experimental strategy (bottom left). Shown are example pseudocolor images (top) and traces (bottom) of the evoked change in OT1.0 and iGluSnFR fluorescence in ACSF, the L-type VGCC blocker nimodipine (Nim; 10 μM), the P/Q-type VGCC blocker ω-Agx-IVA (0.3 μM), the N-type VGCC blocker ω-CTx-GVIA (1 μM) or 200 μM Cd^{2+} to block all VGCCs (slices were sequentially perfused with the indicated blockers). **d**, Normalized peak responses for the data measured in **c**; $n = 4$ slices from 2 mice for OT1.0 and $n = 4$ slices from 2 mice for iGluSnFR. Paired two-tailed Student's *t* tests: $P = 7.6 \times 10^{-3}$, 9.8×10^{-3}, 2.5×10^{-3} and 3.2×10^{-3} (left); $P = 0.075$, 3.6×10^{-3}, 1.1×10^{-3} and 0.20 (right) (between ACSF, nimodipine, ω-Agx, ω-CTx and Cd^{2+}). **e**,**f**, Same as **c** and **d**, respectively, for OT1.0 and iGluSnFR expressed in the PVN; $n = 7$ slices from 3 mice for OT1.0 and $n = 5$ slices from 3 mice for iGluSnFR. Paired two-tailed Student's *t* tests: $P = 0.41$, 3.8×10^{-3}, 1.8×10^{-3} and 4.4×10^{-4} (left); $P = 0.041$, 0.065, 0.18 and 0.08 (right) (between ACSF, ω-Agx, ω-CTx, nimodipine and Cd^{2+}). $^{*}P < 0.05$, $^{**}P < 0.01$, $^{***}P < 0.001$; NS, not significant. All scale bars represent 100 μm. Summary data are presented as the mean ± s.e.m.

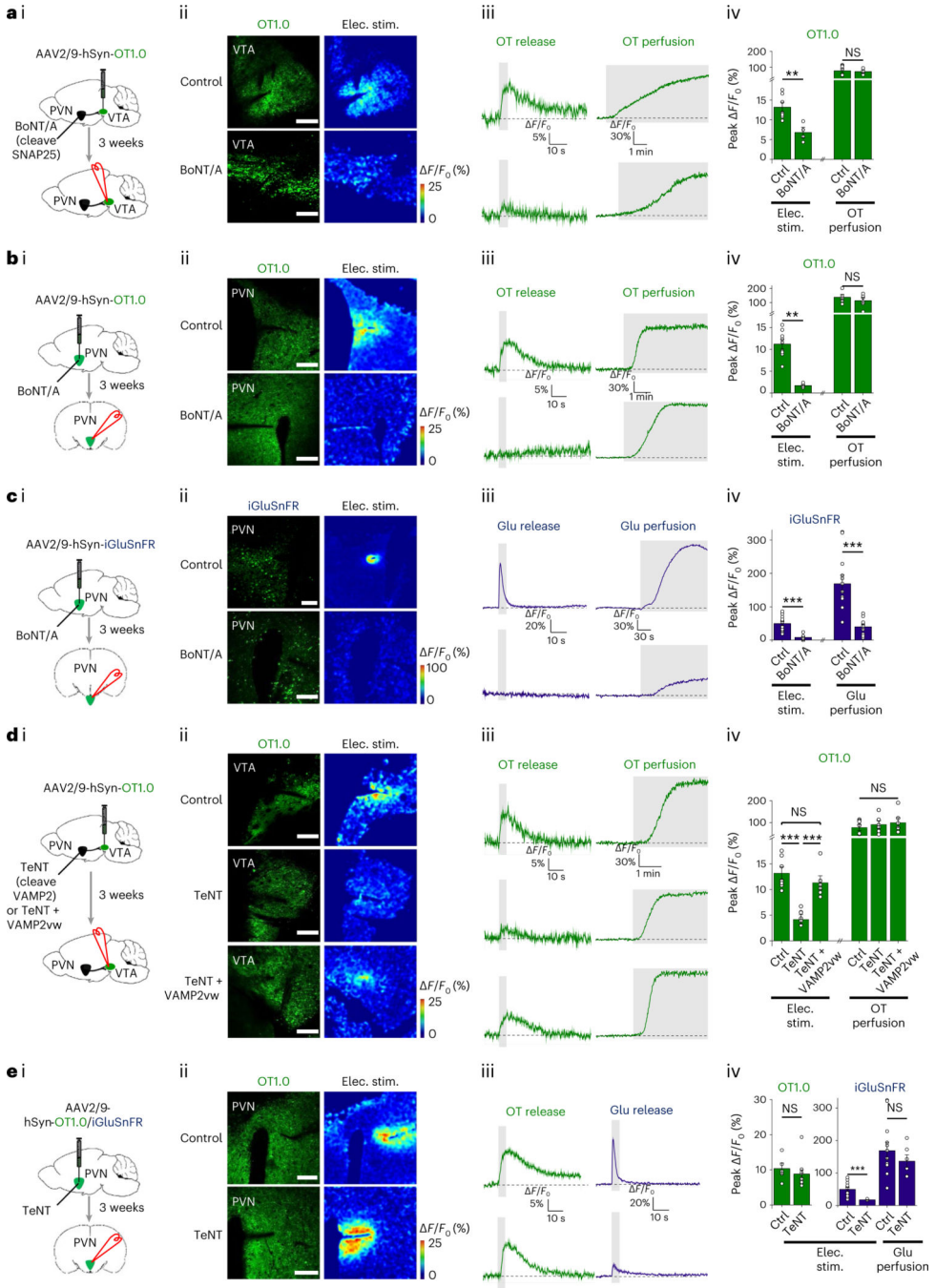

Fig. 4 |. SNARE proteins have distinct roles in axonal and somatodendritic OT release.

a–**e**, Schematic drawings depicting the experimental strategy (i), representative images showing the expression and peak response of the OT1.0 sensor or iGluSnFR (ii), average traces (iii) and summary (iv) of OT1.0 and/or iGluSnFR in response to a 100-pulse stimulation delivered at 20 Hz or OT or glutamate perfusion applied under the indicated conditions. For the summary data, in control (Ctrl) groups, $n = 9$ slices from 6 mice (9/6) (**a**,**d**), 5/4 (**b**,**e**) and 12/4 (**c**,**e**) for OT1.0 in the VTA and PVN and iGluSnFR in the PVN; in BoNT/A groups, $n = 4/2$ (**a**), 6/2 (**b**) and 9/3 (**c**) for OT1.0 in the VTA and PVN and

iGluSnFR in the PVN; in TeNT groups, $n = 8/4$ (**d**), 11/4 (**e**) and 6/2 (**e**) for OT1.0 in the VTA and PVN and iGluSnFR in the PVN; and in the TeNT + VAMP2vw group, $n = 6/3$ (**d**). Two-tailed Student's t tests: $P = 2.3 \times 10^{-3}$ (left) and 0.24 (right) (**a**); $P = 5.3 \times 10^{-3}$ (left) and 0.39 (right) (**b**); $P = 2.5 \times 10^{-5}$ (left) and 3.6×10^{-4} (right) (**c**); $P = 3.8 \times 10^{-6}$, 9.1×10^{-4}, 0.18 (left) and 0.89, 0.76, 0.84 (right) (between Ctrl and TeNT, TeNT and TeNT + VAMP2vw, TeNT + VAMP2vw and Ctrl) (**d**); $P = 0.46$ (left), 3.4×10^{-4} (middle) and 0.18 (right) (**e**). $^{**}P < 0.01$, $^{***}P < 0.001$; NS, not significant. All scale bars represent 100 μm. Summary data are presented as the mean ± s.e.m.

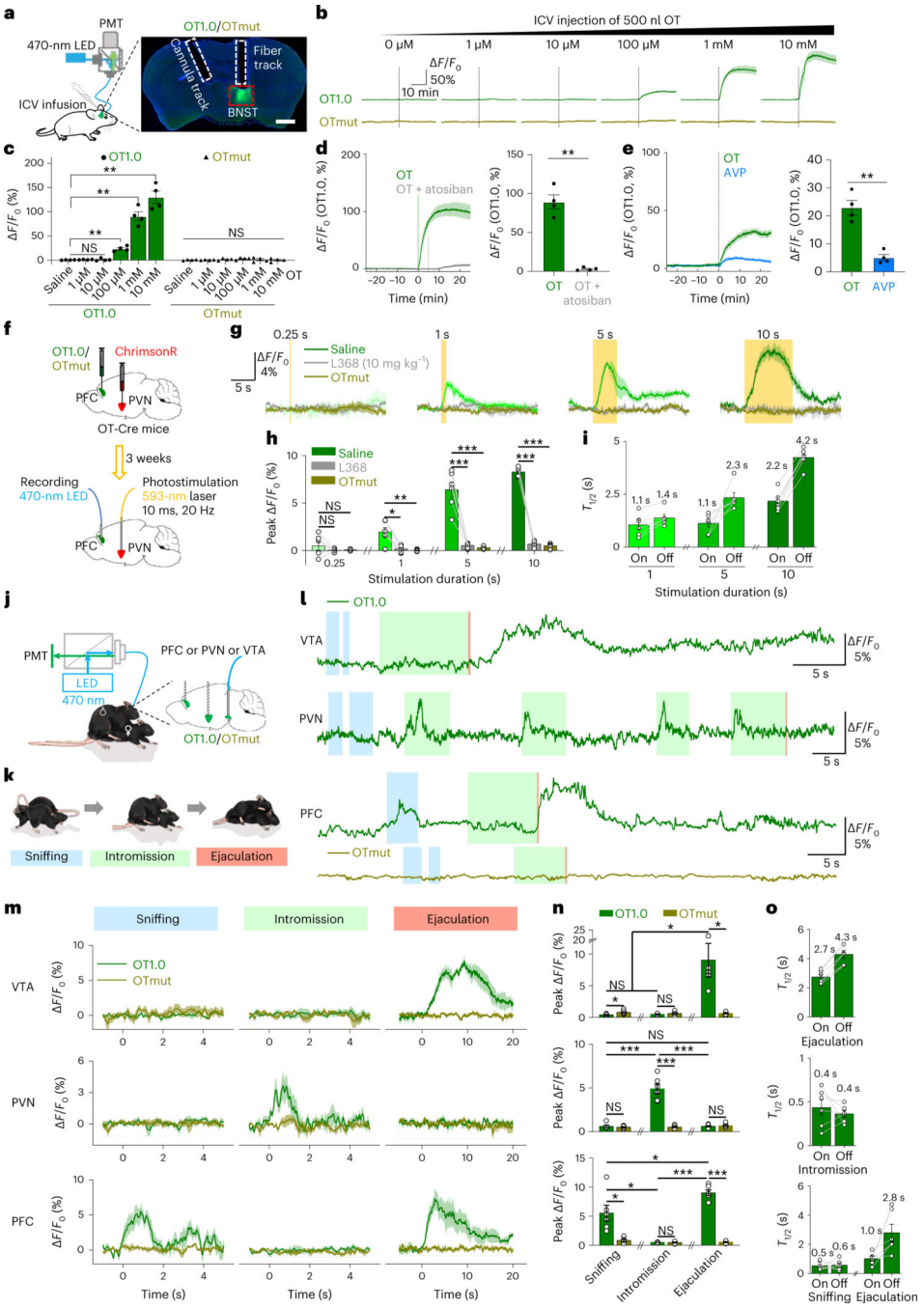

Fig. 5 |. OT1.0 can be used to monitor OT release in vivo during male mating.

a, Schematic illustrations depicting the in vivo intracerebroventricular (ICV) infusion experiments (left) and a fluorescence image of OT1.0 expressed in the BNST (right). Scale bar, 1 mm. **b**,**c**, Averaged traces (**b**) and summary (**c**) of the change in OT1.0 or OTmut fluorescence in response to the indicated concentrations of OT in mice. $n = 4$ mice per group. Paired two-tailed Student's t tests: OT1.0: $P = 0.20$, 0.75, 2.8×10^{-3}, 2.4×10^{-3} and 2.1×10^{-3}; OTmut: $P = 0.91$, 0.26, 0.12, 0.80 and 0.95 (between saline and 1 μM, 10 μM, 100 μM, 1 mM and 10 mM OT). **d**, Averaged traces (left) and summary (right) of $\Delta F/F_0$ in

OT1.0- expressing mice in response to the application of 500 nl of 1 mM OT with or without (reused from **b**) 500 nl of 50 mM atosiban. $n = 4$ mice per group. Two-tailed Student's t test, $P = 2.3 \times 10^{-3}$. **e**, Averaged traces (left) and summary (right) of $\Delta F/F_0$ in OT1.0-expressing mice in response to the application of 500 nl of 100 μM OT (reused from **b**) or 500 nl of 100 μM AVP. $n = 4$ mice per group. Two-tailed Student's t test, $P = 2.7 \times 10^{-3}$. **f**, Schematic illustrations depicting the optogenetic activation experiments. **g**,**h**, Averaged traces of five trials (**g**) and peak response summary (**h**) of OT1.0 and OTmut in the PFC following photostimulation of the PVN in OT-Cre mice that received an intraperitoneal injection of saline or L368. In **h**, $n = 6$ mice per group. Paired two-tailed Student's t tests were performed between saline and L368: $P = 0.39$, 0.014, 8.6×10^{-4} and 1.1×10^{-6} for 0.25, 1, 5 and 10 s, respectively. Two-tailed Student's t tests were performed between saline and OTmut: $P = 0.41$, 8.5×10^{-3}, 5.8×10^{-4} and 1.4×10^{-6} for 0.25, 1, 5 and 10 s, respectively. **i**, Summary of the rise and decay time constants ($T_{1/2}$) of the optogenetically evoked OT1.0 response; $n = 6$ mice per group. **j**, Schematic diagram depicting the experimental strategy for in vivo recording of OT1.0 in mice. **k**, Cartoon illustration of the three principal behaviors during male mating. **l**–**o**, OT1.0 or OTmut $\Delta F/F_0$ measured in the VTA (top), PVN (middle) or mPFC (bottom) during male mating. Shown are representative traces of a single recording (**l**), average time-locked traces from five individual behaviors (**m**), a summary of the peak responses (**n**) and the time constants (**o**) measured during the indicated mating behaviors; $n = 6$ mice per group. Two-tailed Student's t tests were performed between OT1.0 and OTmut for each region: $P = 0.031$, 0.45 and 0.024; 0.51, 4.2×10^{-4} and 0.56; and 0.017, 0.67 and 7.6×10^{-6} for VTA, PVN and PFC, respectively. Paired two-tailed Student's t tests were performed between sniffing and intromission, between sniffing and ejaculation and between intromission and ejaculation for each region: $P = 0.23$, 0.021 and 0.023; 9.3×10^{-4}, 0.99 and 6.1×10^{-4}; and 0.014, 0.045 and 1.1×10^{-5} for VTA, PVN and PFC, respectively. $^{*}P < 0.05$, $^{**}P < 0.01$, $^{***}P < 0.001$; NS, not significant. Summary data are presented as the mean ± s.e.m.

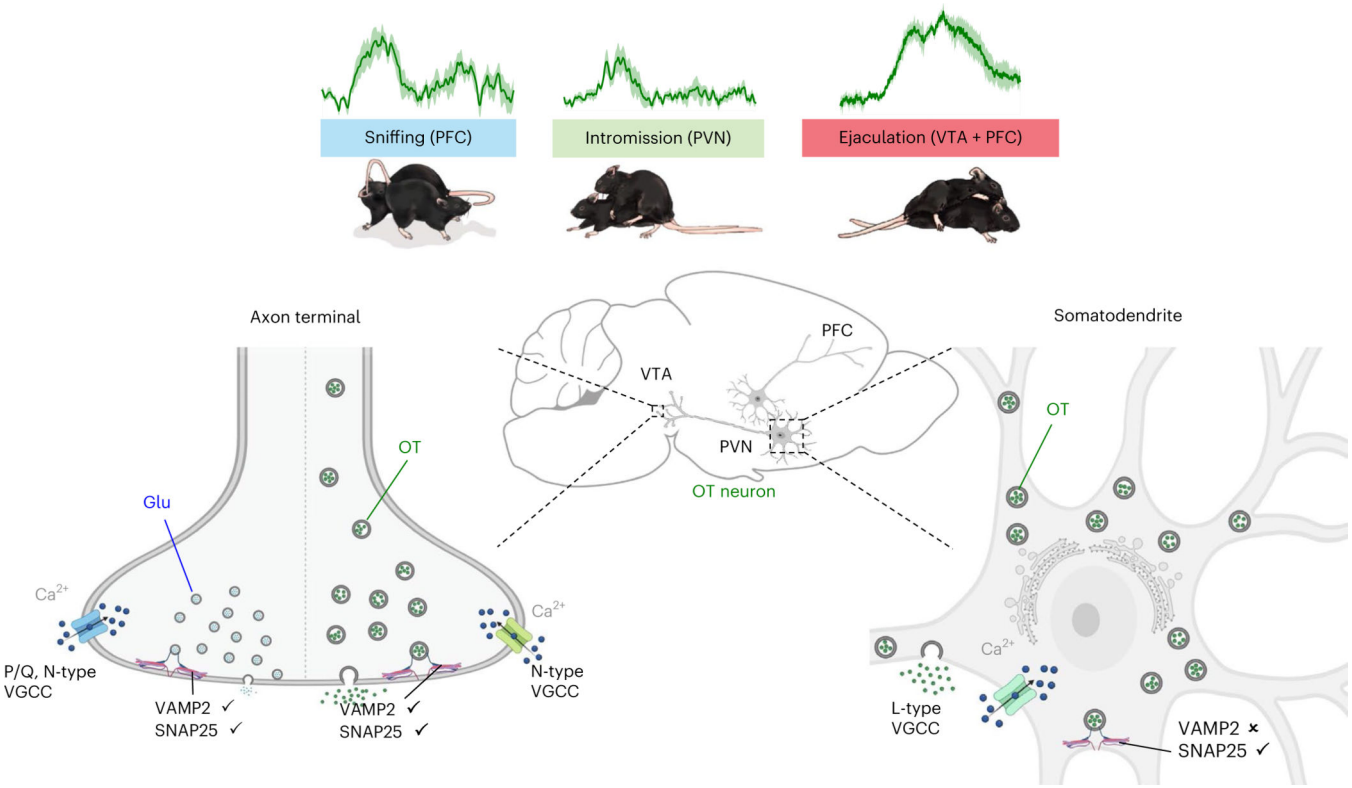

Fig. 6 |. Model showing the molecular basis for axonal versus somatodendritic OT release.
In the male brain during mating, OT is released from different compartments and via different mechanisms during the various behaviors. Top, during sniffing, OT is released primarily from the mPFC; during intromission, OT is released from the PVN; and, finally, during ejaculation, OT is released from the VTA and mPFC. Bottom, axonal OT release is mediated primarily by N-type VGCCs and the SNARE proteins SNAP25 and VAMP2 (left). In contrast, somatodendritic OT release is mediated primarily by L-type VGCCs and SNAP25, but does not require VAPM2 (right). Note that the release of classic neurotransmitters such as glutamate from small presynaptic vesicles is mediated by P/Q-type VGCCs, N-type VGCCs, SNAP25 and VAMP2.